Bhattacharya, Atmadeep; Shahanaghi, Ali; Kaario, Ossi; Vuorinen, Ville; Tripathi, Rupali; Sarjovaara, Teemu

Effects of blending 2,5-dimethylfuran and dimethyl ether to toluene primary reference fuels

Published in:
Fuel

DOI:
10.1016/j.fuel.2021.121401

Published: 15/11/2021

Document Version
Publisher's PDF, also known as Version of record

Please cite the original version:
Bhattacharya, A., Shahanaghi, A., Kaario, O., Vuorinen, V., Tripathi, R., & Sarjovaara, T. (2021). Effects of blending 2,5-dimethylfuran and dimethyl ether to toluene primary reference fuels: A chemical kinetic study. *Fuel*, *304*, Article 121401. https://doi.org/10.1016/j.fuel.2021.121401

Fuel 304 (2021) 121401

Contents lists available at ScienceDirect

Fuel

journal homepage: www.elsevier.com/locate/fuel

Full Length Article

Effects of blending 2,5-dimethylfuran and dimethyl ether to toluene primary reference fuels: A chemical kinetic study

Atmadeep Bhattacharya [a,*], Ali Shahanaghi [a], Ossi Kaario [a], Ville Vuorinen [a], Rupali Tripathi [b], Teemu Sarjovaara [b]

[a] *Department of Mechanical Engineering, Aalto University School of Engineering, Otakaari 4, 02150 Espoo, Finland*
[b] *Neste Corporation Technology Centre, POB 310, 06101 Porvoo, Finland*

ARTICLE INFO

Keywords:
Gasoline combustion knock
2,5-dimethylfuran and dimethyl ether
Chemical kinetic modeling
Soot
Octane number

ABSTRACT

In the present work, renewable oxygenates 2,5-dimethylfuran (DMF) and dimethyl ether (DME) are considered as alternatives to fossil fuels for gasoline engines. The effects of blending DMF and DME on the combustion of gasoline surrogate are numerically studied. The gasoline surrogate is toluene primary reference fuel (TPRF) mixtures containing *iso*-octane, *n*-heptane, and toluene. Two skeletal mechanisms are proposed for the analysis: mechanism A with 504 species and 4212 reactions and mechanism B with 153 species and 740 reactions. These mechanisms are validated against a wide range of experimental data on ignition delay times and 1-D flames. The main findings of the present work are: 1) The ignition inhibiting effect of DMF dominates over the promoting effect of DME at 750 K and 25 bar when the total mole fraction of DMF and DME is less than 20 %. On the contrary, DME augments ignition with greater strength than the inhibition effect of DMF at 825 K and 25 bar. These observations are made for equimolar mixture of DMF and DME blended with TPRF in varying proportions. 2) The laminar burning velocity change stays within 10% of TPRF-air values for 50% TPRF/25%DMF/25%DME-air mixture for $0.6 \leq \varphi \leq 1.\ 6$. 3) DME mitigates additional soot emission caused by DMF blending with TPRF. 4) For the first time in literature, it is shown that the laminar burning velocity and the maximum slope of $O\dot{H}$ mole fraction in the stoichiometric flames vary linearly with the research octane number (RON) for TPRF-air mixtures.

1. Introduction

The essential role of internal combustion engines in transportation sector together with increasing concerns about anthropogenic carbon emissions make the engine and fuel development a great challenge [1]. Some of the conventional methods to improve the performance of gasoline engines include downsizing (through turbocharging and elevated compression ratio) and using exhaust gas recirculation. Moreover, the use of fossil based gasoline must be alleviated by a gradual shift towards renewable fuels for decoupling the transportation sector from greenhouse gas emissions [2]. To achieve this dual objective of engine efficiency improvement and the augmentation of renewable fuel utilization, clear understanding of the combustion of gasoline blended with novel biofuels is required.

Gasoline is primarily a mixture of six (paraffins, isoparaffins, olefins, naphthenes, aromatics, and oxygenates) classes of chemical compounds [3]. Therefore, modeling the gasoline combustion process accurately is a complicated task. Simplistic surrogate blends are required to understand the phenomena inside the engine cylinder while keeping the computational cost acceptable [4]. The simplest and popularly used gasoline surrogates are the binary mixtures of *iso*-octane and *n*-heptane, denoted as primary reference fuels (PRF) where the amount of *iso*-octane is proportional to the octane number of the gasoline. However, the octane numbers of gasoline are represented by the Research and Motor Octane Numbers (RON and MON). This necessitates the addition of an aromatic compound (like toluene) to the PRF blend so that the octane sensitivity (OS = RON - MON) is non-zero [5]. It has recently been observed that the presence of olefin (diisobutylene) in TPRF blend increases the reactivity by a small but significant amount at temperatures higher than 900 K [6]. This fact enables better prediction of in-cylinder conditions for homogeneous charge compression ignition (HCCI) [6] and turbulent jet ignition (TJI) engines [7]. However, the toluene primary reference fuel (TPRF) (Fig. 1) emulates the aromatic, *n*-paraffinic, and *iso*-paraffinic content in real gasolines, and these three classes encompass more

---

* Corresponding author.
E-mail address: atmadeep.bhattacharya@aalto.fi (A. Bhattacharya).

https://doi.org/10.1016/j.fuel.2021.121401
Received 19 March 2021; Received in revised form 20 June 2021; Accepted 6 July 2021

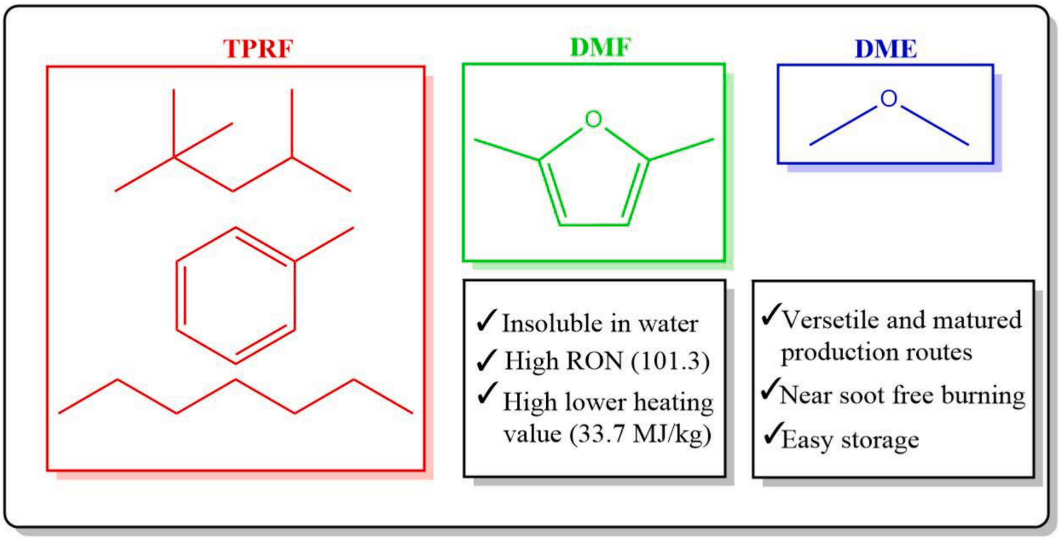

Fig. 1. Fuel molecules and the advantages of DMF and DME considered in the present work.

Table 1
Some detailed and skeletal mechanisms of gasoline surrogate, DMF, and DME in literature.

Type	Reference	No. of Species	No. of Reactions	Initial Mechanism
		Gasoline Surrogates		
Detailed	Curran et al. [41]	990	4060	–
	LLNL [42,43]	1389	9603	–
	CRECK [20]	621	27,369	–
	Andrae [44]	1121	4961	–
	Puduppakkam et al. [45]	1833	8764	–
Skeletal	Cai and Pitsch [46]	339	2791	Curran et al. [41]
	Mehl et al. [47]	312	~1500	LLNL [42,43]
	Givler et al. [48]	110–123	488–502	LLNL [42,43]
Reduced	Wolk and Chen [49]	96	92	LLNL [42,43]
	Chen et al. [50]	107	102	LLNL [42,43]
		DMF		
Detailed	Sirjean et al. [22]	294	1456	–
	BL [23–25]	305	1472	–
	Somers et al. [26]	545	2768	–
		DME		
Detailed	Dagaut et al. [51]	55	331	–
	Curran et al. [52]	78	336	–
	Zhao et al. [33]	55	290	–
Skeletal	Bhagatwala et al. [32]	39	175	Zhao et al. [33]

than 90% of the constituents in real fuel [8]. Therefore, TPRF blends are the most common gasoline surrogates in literature for combustion chemistry studies [4].

In the context of renewable fuels, the use of 2,5-dimethylfuran (DMF) (Fig. 1) as a biomass derived alternative to gasoline has gained increased attention ever since a possible route of its mass production from fructose (a carbohydrate obtained directly from biomass or through the isomerization of glucose) was reported by Román-Leshkov et al. [9]. It has recently been mentioned by Qian et al. [10] that DMF has a high research octane number (RON = 101.3). Therefore, the knocking propensity measurements conducted by Rothamer et al. [11] revealed augmentation in knock resistance for gasoline/DMF blend compared to pure gasoline case. Due to high octane number and insolubility with water, DMF has recently been considered among the top ten biofuel candidates for SI engines [12]. On the other hand, dimethyl ether (DME) is a second-generation biofuel that can also be produced from lignocellulosic biomass. Moreover, DME (Fig. 1) is a non-toxic ether compound that can be stored in a simpler manner compared to other gaseous biofuels due to its ability to liquify at pressures above 5 bar. To exploit these benefits, Shi et al. [13–15] recently published a series of experimental works on the application of DME in gasoline engines. Similarly, Ji et al. [16] reported that the thermal efficiency increases while NO_x and unburnt hydrocarbon (HC) emissions decrease with the addition of DME in a spark ignition (SI) engine run on gasoline. However, the ratio of DME to be blended with gasoline is restricted to small values due to its high cetane number [16].

The simulation of gasoline combustion and other novel biofuels necessitate the development of chemical kinetic mechanisms [4]. Some of the well accepted detailed models on gasoline surrogates are listed in Table 1. However, as pointed out by Lu and Law [17], the overall computational cost of a typical transient computational fluid dynamics (CFD) simulation involving combustion kinetics is a cubic function of the number of species in the mechanism. This fact renders the use of detailed chemical kinetic models infeasible for most internal combustion engine simulations involving CFD. Therefore, skeletal mechanisms that are applicable in a specific parametric range due to their reduced size [18] are constructed. Some of the recently developed skeletal gasoline surrogate mechanisms are mentioned in Table 1 as well. Apart from the mechanisms listed in Table 1, Bhattacharya et al. [19] recently developed a skeletal chemical kinetic mechanism with only 108 species and 1605 reactions for 6 component gasoline surrogates. In this work, the detailed mechanism from CRECK Modeling Group at Politecnico di Milano [20] was reduced using the directed relation graph with error propagation (DRGEP) method [21].

For DMF combustion, there are currently three detailed models [22–26] available in the literature (Table 1). Recently, Weber et al. [27] have studied the pyrolysis of DMF using a modified version of the Bielefeld University and Université de Lorraine (BL) model [23–25]. Furthermore, these detailed mechanisms [22–26] have been utilized to propose many recent mechanisms for gasoline/DMF blends. For example, Eldeeb and Akih-Kumgeh [19] proposed a detailed chemical kinetic mechanism for *iso*-octane/DMF blends. Bhattacharya et al. [28] and Liu et al. [29] published skeletal mechanisms for DMF blends with *iso*-octane and TPRF respectively. These skeletal models [19,29] are based on the detailed mechanism of Somers et al. [26]. On a similar note, the BL model [23–25] has also been augmented with the polycyclic aromatic hydrocarbon (PAH) [30] and TPRF sub-models [31].

Finally, some of the eminent chemical kinetic mechanisms for DME combustion are mentioned in Table 1. As shown in the table, Bhagatwala et al. [32] have reduced the Zhao et al. [33] model into a skeletal version

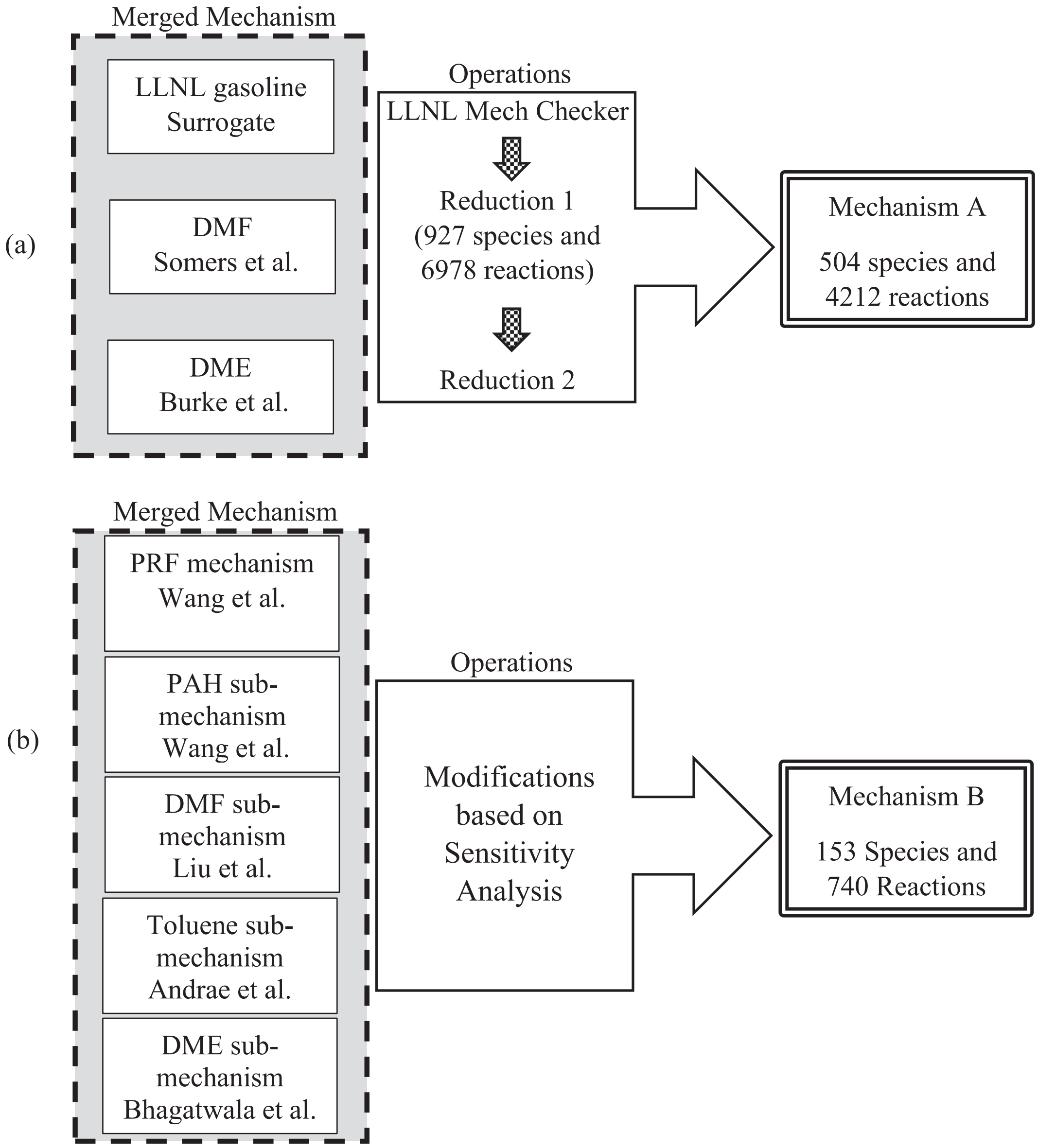

Fig. 2. Schematic explanation of mechanism formation process.

using directed relation graph (DRG) [34] and DRG-aided sensitivity analysis (DRGASA) [35,36]. Recently, there has been some works on the development of chemical kinetic models of fuel blends involving DME. For example, Burke et al. [37] recently proposed a detailed mechanism for methane/DME blend. This model [37] was based on the $C_1 - C_2$ hydrocarbon chemistry from Metcalfe et al. [38]. Subsequently, the Burke et al. [37] mechanism was adopted by Dames et al. [39] for the formulation of a kinetic model containing propane and DME. Zeng et al. [40] proposed a skeletal mechanism for *iso*-octane/DME mixtures with 379 species and 1931 reactions. It has been shown in this work [40] that DME has the potential to reduce soot emission from premixed *iso*-octane-oxidizer flames.

It is clear from the above literature review that there is a plethora of mechanisms for gasoline surrogates. Moreover, considerable amount of work has been done on the combustion kinetics of binary blends involving gasoline/DMF [28,29,53] and gasoline/DME [40]. Despite DME being a viable biofuel candidate for gasoline engines, the chemical kinetic effects of blending DME to gasoline/DMF blend have not been explored yet. In such a blend, the potential loss in octane rating due to DME blending may be compensated by the presence of DMF. The gasoline surrogates involving *iso*-octane, *n*-heptane, and toluene have been considered in the present work. It has been mentioned by Sarathy et al [4] that the TPRF surrogates can successfully capture the autoignition and laminar burning characteristics of a wide variety of gasoline fuels. The objectives of the present work are,

1. Formulation and validation of chemical kinetic mechanisms for TPRF/DMF/DME blends in the SI engine context
2. Analysis of the variation of ignition delay time and laminar burning velocity due to DMF and DME blending in TPRF
3. Chemical kinetic analysis of soot formation in 1-D flames involving TPRF/DMF/DME blends
4. Investigation of the chemical kinetics of TPRF surrogate mixtures in 1-D flames and its implication on octane rating

2. Mechanism formulation methodology

This section describes the procedures adopted in the present work for the formulation of chemical kinetic schemes suitable for the analysis of premixed flames involving TPRF/DMF/DME blends. The mechanism formation process adopted in this work is summarized in Fig. 2 (a-b). First, a semi-detailed mechanism containing 504 species and 4212

Table 2
Conditions used in the formation process of mechanism A.

Reduction 1
• Tool: PyMARS • Isochoric batch reactor simulations for *iso*-octane, *n*-heptane, toluene, DMF, and DME-air mixtures • Conditions: • DRGEP • Pressure: 10 bar • Temperaturers: 650 K, 750 K, 850 K, 1000 K, 1100 K • $\varphi = 1$ • Target: • Species profiles: OH, H, H_2O_2, HO_2, *iso*-octane, *n*-heptane, toluene, DMF, and DME • Allowed error on target: 5 %
Reduction 2
• Tool: PyMARS • Isochoric batch reactor simulations for *iso*-octane, *n*-heptane, toluene, DMF, and DME-air mixtures • Conditions: • DRGEP • Pressure: 10 bar • Temperaturers: 650 K, 750 K, 850 K, 1000 K, 1100 K • $\varphi = 1$ • Target: Species profiles: OH, H, H_2O_2, HO_2 • Allowed error on target: 10 %

reactions (namely mechanism A) has been formulated (Fig. 2 (a)). However, this mechanism is computationally expensive due to its large size. Therefore in the second step, another skeletal mechanism with 153 species and 740 reactions (namely mechanism B) has been prepared as the final step of the mechanism development process (Fig. 2 (b)).

As seen from Table 1, the LLNL detailed gasoline surrogate model [42] is well accepted and is the basis for numerous skeletal mechanisms published recently. Therefore, the starting point for the gasoline surrogate combustion chemistry has been chosen to be the semi-detailed LLNL mechanism for gasoline surrogate [42] containing 679 species and 5627 reactions. This mechanism was reduced from the detailed one containing 1389 species and 9603 reactions. The methods described in [17] targeting *iso*-octane, *n*-heptane, toluene, 2-pentene, and ethanol as pure components and their mixtures were used for the reduction process.

As shown in Fig. 2 (a), the DME sub-model from Zhang et al. [54] and the sub-model for DMF from Somers et al. [26] have been merged into the gasoline surrogate mechanism to obtain a detailed tri-fuel mechanism with 1244 species and 7584 reactions. After the formation of the detailed tri-fuel mechanism, the discontinuities in the species thermodynamic properties (i.e. the NASA polynomial coefficients for heat capacity, enthalpy, and entropy) have been removed using the open-source tool LLNL Mech Checker (https://combustiontools.llnl.gov/). Following the fixing of discontinuous thermodynamic data, a two-step strategy has been adopted for the reduction of this detailed tri-fuel mechanism. The python based open-source automatic mechanism reduction tool pyMARS [55] has been implemented in this work. Transient species profiles from the isochoric batch reactor simulations have been used as targets for the reductions.

The details of the parametric conditions adopted in pyMARS for mechanism reduction process are given in Table 2. In the initial phase of reduction, stoichiometric fuel–air mixtures involving *iso*-octane, *n*-heptane, toluene, DMF, and DME have been considered at 10 bar pressure and temperature range 650-1100 K. This temperature range ensures the coverage of both low and high temperature chemical kinetic domains. The primary objective behind this initial reduction phase is to exclude the higher molecular weight species that are specific to the fuel decomposition. Therefore, the target parameters are chosen to be the transient profiles of the fuel species along with the intermediates like H, OH, H_2O_2, and HO_2 with a narrow error margin of 5%. The DRGEP reduction algorithm [21] has been used. In DRGEP, redundant species are identified iteratively until a user specified error limit is reached between the predicted and the target parameters. As seen from Fig. 2 (a), this reduction phase resulted in a skeletal mechanism for TPRF/DMF/DME blend with 927 species and 6978 reactions.

The second phase of reduction process starts with the mechanism containing 927 species and 6978 reactions as input (Fig. 2 (a)). Similar to the earlier phase, the reduction algorithm used in this phase is DRGEP [24]. Moreover, as seen from Table 2, the input fuel–air mixtures, pressure, and temperature range are same as the earlier phase. However, the main objective behind this reduction process is the exclusion of smaller intermediates that are of minor importance towards the calculation of ignition delay time. Therefore, the second phase has fewer target parameters, i.e. the transient profiles of the intermediates H, OH, H_2O_2, and HO_2. The error limit has been increased to 10% for this phase. This reduction operation resulted in the formation of the mechanism containing 504 species and 4212 reactions (mechanism A). This mechanism (available in supplementary material) has been validated and adopted for 0-D batch reactor simulations in the present work.

Any further reduction in mechanism A resulted in large errors in target parameters. Therefore, another skeletal mechanism has been formed in the present work. A description of this mechanism formulation approach can be seen in Fig. 2 (b). As seen from the figure, the starting point for this skeletal mechanism development process has been chosen to be the TPRF/DMF/PAH mechanism by Liu et al. [29] containing 136 species and 617 reactions. It is important to note in this regard that this mechanism [29] contains many sub-mechanisms of the relevant fuel and pollutant species,

1) The PRF and toluene sub-mechanisms [56,57] belong to skeletally reduced versions of the detailed LLNL mechanism [42].
2) The PAH sub-mechanism [58]—containing up to four aromatic rings, i.e. pyrene (A_4)—has been reduced from the detailed mechanism proposed by Slavinskaya et al. [59].
3) The DMF sub-mechanism [29] has been skeletally reduced from the detailed mechanism of Somers et al. [26].

It may be seen from the work of Wang et al. [56,57] that the PRF sub-mechanism has been validated against a wide range of experimental data on laminar flames, shock tube species profiles, well stirred reactor, ignition delay times—at low, intermediate, and high temperature region—and pressure–time histories in HCCI engine. Similar experimental data have been used for the validation of the DMF sub-mechanism [29] as well. Moreover, Liu et al. [29] have validated the prediction of soot precursors (like acetylene (C_2H_2) and benzene (C_6H_6)) by their TPRF/DMF/PAH mechanism for the pyrolysis and oxidation of DMF.

First, the extension of TPRF/DMF/PAH mechanism [29] has been done by adding the DME breakup pathway from the skeletal mechanism of Bhagatwala et al. [32]. The DME breakup pathway adopted in the present study contains 56 reactions among 16 species. A list containing these reactions is provided in Table S1 of the supplementary material. It may be seen from Table S1 that the DME breakup pathway primarily involves reactions that are part of the H_2/C_1 core chemistry. Furthermore, the strong dependence of laminar burning velocity (S_L) of hydrocarbon fuels on the H_2/C_1 core chemistry is a well-known fact [4].

Next, the repercussions of the addition of DME chemistry to the TPRF/DMF/PAH mechanism has been assessed through the evaluation and comparison of laminar burning velocity values for individual fuel components, i.e. *iso*-octane, *n*-heptane, toluene, and DMF with experimental data from literature. It was found that the addition of DME chemistry had little influence on the laminar burning velocity of *iso*-octane, *n*-heptane, and DMF. However, the laminar burning velocity of toluene-air mixtures was found to be severely affected by the added H_2/C_1 core chemistry in the DME mechanism. It has recently been explained by Yang et al. [60] that the toluene combustion mechanism is more sensitive —than alkanes—to the H_2/C_1 core chemistry because (a) the

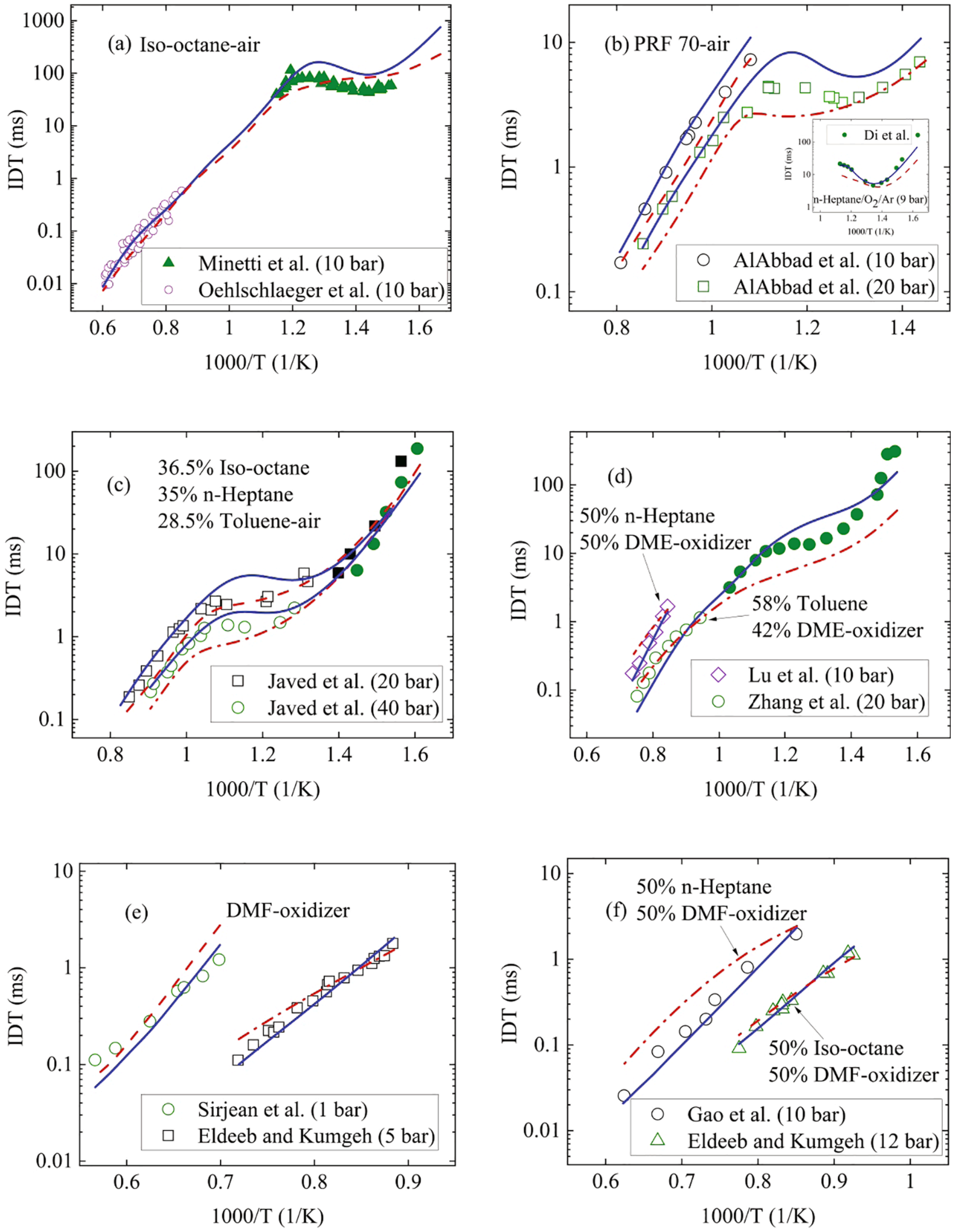

Fig. 3. Comparison of performance of mechanism A (bold lines) and mechanism B (dotted lines) in predicting the experimental data (symbols) on ignition delay time (IDT) from (a) Minetti et al. [68] and Oehlschlaeger et al. [69], (b) AlAbbad et al. [73] and Di et al. [74] (inset), (c) Javed et al. [75], (d) Zhang et al. [76] and Lu et al. [77], (e) Eldeeb and Kumgeh [53] and Sirjean et al. [22], and (f) Eldeeb and Kumgeh [53] and Gao et al. [78]. Filled symbols represent data from RCM and hollow symbols represent data from ST at stoichiometric condition.

decomposition of its aromatic structure involves more complicated chemical network and (b) the high-temperature mechanism has a greater influence on the fundamental combustion parameters like ignition delay time and laminar burning velocity.

An example of the deviation of the merged mechanism predictions from the experimental data is shown in Fig. S1 of the supplementary material for unburnt gas temperature of 298 K at atmospheric pressure. The experimental data shown in Fig. S1 has been taken from Dirrenberger et al. [61] and Hirasawa et al. [62]. It may be seen from the figure that the merged mechanism (a) underpredicts the experimental data from Dirrenberger et al. [61] for $\varphi \leq 1.1$ and (b) overpredicts the experimental data from Hirasawa et al. [62] for $\varphi \geq 1.1$. The equivalence ratio corresponding to the peak laminar burning velocity is also shifted to $\varphi = 1.2$. It can be noted here that Dirrenberger et al. [61] used the heat flux burner method and Hirasawa et al. [62] adopted the counter flow burner for the measurement of laminar burning velocity. Moreover, the heat flux burner method is the most accurate one for the determination of laminar burning velocity at low pressures [63].

To improve the model predictions with respect to the experimental data, a part of the toluene breakup pathway of the initially merged mechanism has been replaced by the same from Andrae et al. [64] (Fig. 2 (b)). This action is motivated by the fact that the preservation of compactness of the mechanism necessitates increased focus on the validation of fundamental combustion characteristics like laminar burning velocity and ignition delay time [60,65]. It may be mentioned in this context that the skeletal mechanism from Andrae et al. [64] has been validated at a wide range of pressures and temperatures against the experimental data on laminar burning velocity and ignition delay time of TPRF-oxidizer mixtures. A list containing the added set of reactions from Andrae et al. [64] is provided in Table S2 of the supplementary material.

After the addition of the toluene breakup reactions, sensitivity analysis has been performed on the laminar burning velocity of toluene-air mixture (Fig. 2 (b)). During the sensitivity analysis, the normalized sensitivity coefficient for a particular reaction 'i' in a chemical mechanism with specific forward reaction rate k_i has been defined as $(k_i/S_L)(\partial S_L/\partial k_i)$. This way, the most important reactions towards the prediction of laminar burning velocity can be identified. As per the suggestions from the sensitivity analysis results, the Arrhenius parameters of the H abstraction reaction $C_6H_5CH_3 + H = C_6H_5\dot{C}H_2 + H_2$ has been adopted from Rao and Skinner [66]. It may be seen from Fig. S1 that the final version of the mechanism—denoted as "mechanism B"—performs well in predicting the experimental data from Dirrenberger et al. [61]. This mechanism contains 153 species and 740 reactions and is provided as supplementary material.

3. Validation of the mechanisms

3.1. Ignition delay time of TPRF/DMF/DME blends

After the formulation of the mechanisms (A and B), the next step is to validate them against the experimental data from literature. A wide range of dataset on ignition delay times (IDTs) of various fuel-oxidizer mixtures has been used for that purpose initially (Fig. 3 (a-f)). The details about the fuel-oxidizer compositions, pressure, and temperature range of the experimental data used in Fig. 3 (a-f) can be found in Table A1 (Appendix A). It is evident from the table that the experimental data include both shock tube (ST) and rapid compression machine (RCM) results. All the simulations of the IDTs in Fig. 3 have been performed using the adiabatic constant volume batch reactor model in Cantera 2.4.0 [67] using the Python interface.

Fig. 3 (a) shows the validation of mechanism A and B against the experimental data [68,69] on IDT of stoichiometric *iso*-octane-air mixture at 10 bar. It is evident from the figure that the IDT is well predicted by both mechanism A and B in the higher temperature range where the IDT decreases with the increase in temperature. It may be observed from Fig. 3(a) that the IDT increases when temperature is increased in the range 700–800 K. This variation is contrary to the general decreasing trend of IDT with increase in temperature below 700 K (low temperature) and above 800 K (high temperature) region. Such observations at intermediate temperature ranges are common for high molecular weight paraffin oxidation processes and are termed in the literature as the negative temperature coefficient (NTC) behavior. While the high temperature oxidation of alkanes rapidly proceeds through the β-scission decomposition of the alkyl radicals ($\dot{R}$), the low temperature pathway is more complex and proceeds through $\dot{R}+O_2 \rightarrow R\dot{O}_2 \leftrightarrow \dot{Q}OOH + O_2 \rightarrow O_2QOOH \leftrightarrow HO_2QOOH \rightarrow R\dot{O} + O\dot{H} + O\dot{H}$ [70]. In the intermediate temperature range, the formation of $R\dot{O}_2$ is not favored. Instead, hydroperoxyl radicals (HO_2) and alkenes are formed through the $\dot{R}+O_2$ reaction. These HO_2 radicals further react with the alkanes to produce H_2O_2. These intermediate species (alkene, HO_2, H_2O_2) decelerate the global rate of oxidation and produce the NTC region due to their stable nature [71,72].

As observed from Fig. 3 (a), the NTC behavior of stoichiometric *iso*-octane-air mixture is accurately predicted by mechanism A. On the other hand, mechanism B predicts a mild occurrence of NTC. The cause of this mild prediction may be attributed to the absence of $\dot{Q}OOH$, $R\dot{O}$, and alkene (C_8H_{16}) species generated from *iso*-octane molecule in mechanism B. It may be noted here that the *iso*-octane sub-mechanism in mechanism B has been adopted from the skeletal mechanism of Wang et al. [56] where $\dot{Q}OOH$, $R\dot{O}$, and alkene (C_8H_{16}) species have been excluded to achieve a mechanism suitable for 3-D CFD applications. On a similar note, the formation and consumption paths of $\dot{Q}OOH$, $R\dot{O}$, and C_8H_{16} have not been included in mechanism B to preserve its brevity in the present work.

For further validation of the mechanisms (A and B), the IDT of stoichiometric PRF 70-air mixture at 10 and 20 bar pressure is shown in Fig. 3 (b). The experimental data are taken from AlAbbad et al. [73]. It may be seen from the figure that the IDT is well predicted by both mechanisms (A and B) in the higher temperature range for 10 and 20 bar pressure. Mechanism B predicts a marginally quicker ignition compared to mechanism A which is closer to the experimental data. Moreover, mechanism A successfully predicts the NTC behavior at 20 bar in Fig. 3 (b). Similar observations can be made from Fig. B1 in Appendix B for PRF 80-air mixture as well. As shown in Table A1, the experimental data [73] have been obtained using a high-pressure shock tube (HPST) facility. At low and intermediate temperature range near NTC region, the HPST apparatus produces a pre-ignition heat release effect [73]. This effect has not been considered in the present isochoric batch reactor simulations. Therefore, the predicted IDT values near the NTC region are longer than the experimental ones (Fig. 3 (b) and B1).

To establish the validity of mechanism A and B in the low temperature and NTC region, the experimental data from Di et al. [74] for 1.34% *n*-heptane/14.89% O_2/83.77% Ar mixture at 9 bar have been used in the inset of Fig. 3 (b). It may be seen from the figure that mechanism B predicts a little shorter IDT for the stoichiometric *n*-heptane-oxidizer mixture. However, as seen from Fig. 3 (a) and inset of Fig. 3 (b), mechanism A can predict the NTC behavior of *iso*-octane and *n*-heptane both qualitatively and quantitatively. On the other hand, the IDTs of 36.5% *iso*-octane/35% *n*-heptane/28.5% toluene-air mixture at 20 and 40 bar have been used for validation in Fig. 3 (c) against the experimental data from Javed et al. [75]. It may be seen from the figure that mechanism A predicts the IDT values at high temperature range quite accurately for the TPRF-air mixture at both pressures. Although there is marginal overprediction of IDT in the NTC region, mechanism A performs acceptably in predicting the IDTs of the TPRF-air mixture in the studied temperature range in Fig. 3 (c) at 20 and 40 bar pressure. For mechanism B, the predictions are better at lower temperatures ($\leq$800 K). However, there is underprediction (around 30–45% at 20 bar) with respect to the experimental data [75] for mechanism B when the temperature is higher than 1000 K.

After validating mechanism A and B for *iso*-octane, PRF and TPRF mixtures, the IDT of stoichiometric 58% toluene/42% DME-oxidizer mixture has been used for comparison in Fig. 3 (d) at 20 bar. The experimental data have been taken from the recently published work of Zhang et al. [76]. Moreover, the recent work of Lu et al. [77] has been adopted as the source of experimental data for 50% *n*-heptane/50% DME-oxidizer mixture on the high temperature IDTs at 10 bar in Fig. 3 (d). It is clear from the figure that in both the cases, mechanism A performs very well in predicting the experimental data. It may be mentioned here that like high molecular weight alkanes, DME also exhibits the NTC behavior. This fact is evident in Fig. 3 (d) for 58% toluene/42% DME-oxidizer mixture. Some deviations from the experimental results are also observed for the predicted values using the smaller mechanism B. A maximum deviation (with experimental data) of 86% is seen for the 58% toluene/42% DME-oxidizer mixture at 650 K and 20 bar. However, for 2.73% DMF/20.43% O_2/76.84% Ar mixture at 5 bar from Eldeeb and Kumgeh [53] and 0.25% DMF/1.875% O_2/97.875% Ar mixture at 1 bar from Sirjean et al. [22], both the mechanisms perform reasonably well in predicting the IDTs at studied temperature range in Fig. 3 (e).

Fig. 3 (f) compares the performance of the mechanisms (A and B) with experimental data from Eldeeb and Kumgeh [53] for 1.05% *iso*-

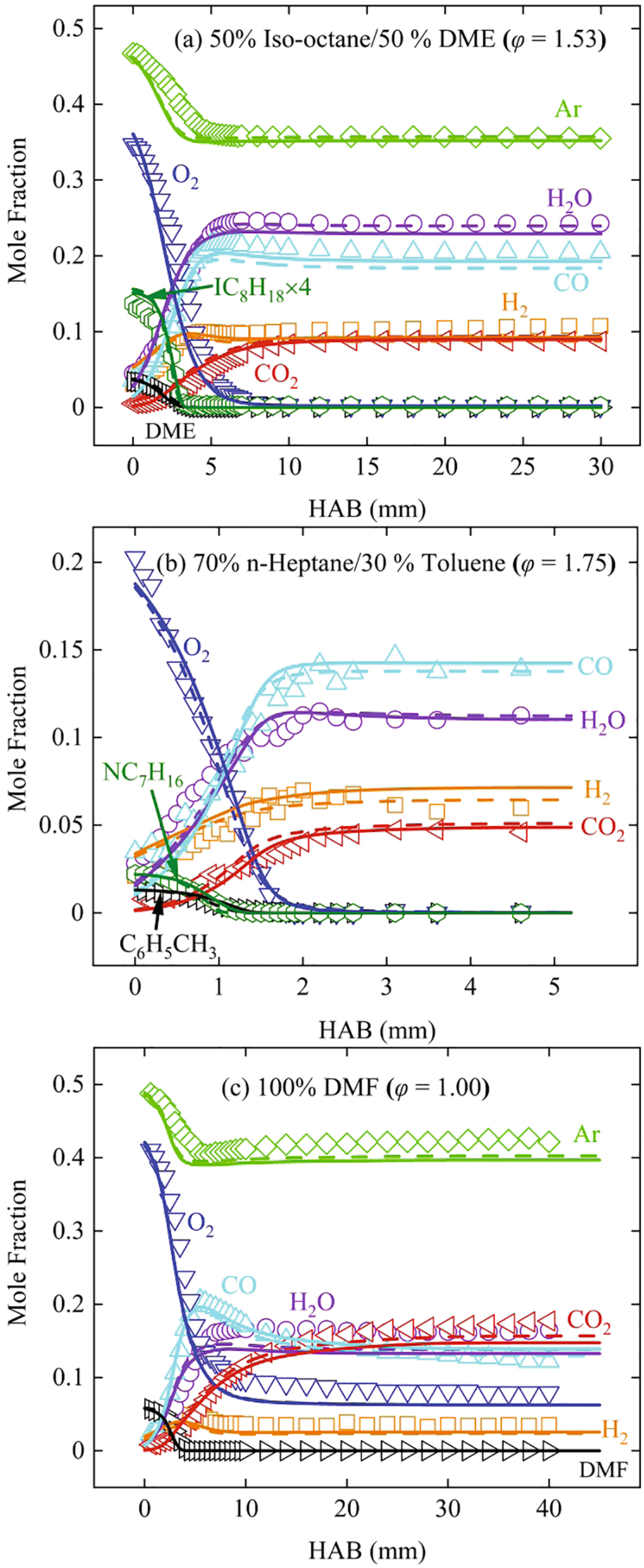

Fig. 4. Comparison of performance of mechanism A (bold lines) and mechanism B (dotted lines) in predicting the major species profile distributions over the height above burner (HAB) for 1-D flames with experimental data (symbols) from (a) Zeng et al. [40], (b) Dmitriev et al. [79], and (c) Togbé et al. [24].

octane/1.05% DMF/20.57% O_2/77.33% Ar mixture at 12 bar and Gao et al. [78] for 0.222% *n*-heptane/0.222% DMF/4.108% O_2/95.448% Ar mixture at 10 bar. It may be seen from the figure that mechanism A provides accurate predictions for both fuel-oxidizer mixtures. On the other hand, although mechanism B provides correct predictions for the IDTs of the 50%*iso*-octane/50% DMF-oxidizer mixture, it predicts slower ignition for the 50% *n*-heptane/50% DMF case in Fig. 3 (f). A maximum deviation (from experimental data) of around 23% can be observed at 1175 K for the 50% *n*-heptane/50% DMF-oxidizer mixture.

Finally, mechanism A and B have been validated at lean stoichiometric condition ($\varphi = 0.5$) in Fig. B2 (a-c) (Appendix B). Fig. B2 (a) compares the performance of the mechanisms with experimental data from Sarathy et al. [8] for fuels for advanced combustion engines (FACE) type C in air at 20 bar pressure. The TPRF surrogate for FACE C gasoline is 34.06% *iso*-octane/12.28% *n*-heptane/53.66% toluene (by mol). Similarly, the experimental data from Eldeeb and Kumgeh [53] for 1.38% DMF/20.72% O_2/77.9% Ar mixture at 12 bar is used in Fig. B2 (b) for comparison. Moreover, the experimental dataset from Zhang et al. [76] has been adopted in Fig. B2 (c) for validating mechanism A and B. The pressure is 20 bar and the unburnt gas mixture contains 58% toluene/42% DME-oxidizer mixture at $\varphi = 0.5$ in Fig. B2 (c). It may be said from an overall perspective that both mechanism A and B perform within the acceptable range for IDT predictions of various fuel blends involving *iso*-octane, *n*-heptane, toluene, DMF, and DME. Moreover, mechanism A perform better than mechanism B in predicting the NTC phenomenon for TPRF and DME.

3.2. Laminar premixed flames of TPRF/DMF/DME blends

The experimentally obtained species profiles from 1-D flames stabilized on flat burners have been used as the next set of validation targets for mechanism A and B in Fig. 4 (a-c). The details about the fuel-oxidizer compositions and pressures for the unburnt gas can be found in Table A1 (Appendix A). The experimentally measured temperature profiles for the 1-D flames have been provided as inputs and only the species conservation equations have been solved using the proposed chemical kinetic mechanisms A and B. The mixture averaged transport properties have been assumed for the species. The 1-D free flame code implemented in Cantera 2.4.0 [67] has been used for the computations through the Python interface. The adaptive grid parameters are ratio = 3, slope = 0.1, and curve = 0.1 for the burner stabilized 1-D flame. The “slope” and “curve” values have been optimized through a grid independence study in an earlier work [19].

Fig. 4 (a) shows the variations of major species along the height above burner (HAB) for 50% *iso*-octane/50% DME blend at $\varphi = 1.53$. The experimental data are taken from Zeng et al. [40]. Fig. 4 (b) shows the major species profiles for 70% *n*-heptane/30% toluene blend at $\varphi = 1.75$. The experimental data are taken from Dmitriev et al. [79]. Similarly, Fig. 4 (c) shows comparison of the performance of mechanism A and B towards predicting the experimentally obtained [24] major species profiles for stoichiometric DMF/O_2/Ar mixture. It may be seen from Fig. 4 (a-c) that the predictions of species distributions, using the new chemical models (A and B) compare quite well with the experimental data from the literature as most of the predicted values are within ± 10% range of the experimental data. The flat profile of the intermediate species (H_2, CO), complete combustion products (CO_2 and H_2O), and inert gas (Ar) sufficiently upstream to the burner indicate chemical equilibrium. It may be seen from Fig. 4 (a-c) that the proposed mechanisms (A and B) predict the equilibrium mole fractions of the major species quite accurately as well for DMF and binary blends of *iso*-octane/DME and *n*-heptane/toluene.

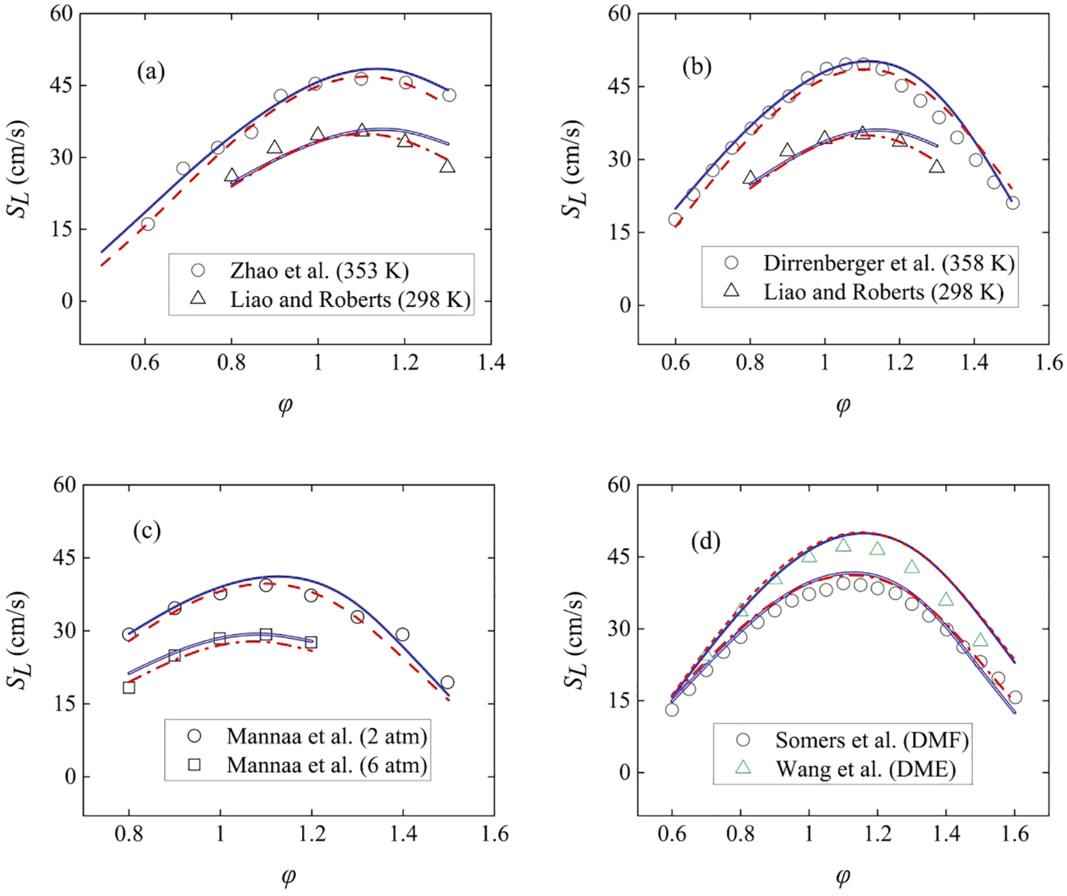

Fig. 5. Comparison of performance of mechanism A (bold lines) and mechanism B (dotted lines) in predicting the experimental data (symbols) on laminar burning velocity from (a) Zhao et al. [80] and Liao and Roberts [81], (b) Dirrenberger et al. [61] and Liao and Roberts [81], (c) Mannaa et al. [82], and (d) Somers et al. [26] and Wang et al. [83]. The details about the unburnt gas compositions, pressures, and temperatures are given in Table A1 (Appendix A).

Next, the comparison of predicted laminar burning velocity using the present mechanisms (A and B) and the experimental data from literature is shown in Fig. 5 (a-d). Fig. 5 (a) shows that the present mechanisms (A and B) predict the experimental data from Zhao et al. [80] for 63% *iso*-octane/17% *n*-heptane/20% toluene (by mol) blend and Liao and Roberts [81] for PRF 95 in air at atmospheric pressure quite accurately for a wide range of equivalence ratios. The unburnt gas temperatures for the TPRF-air mixture from Zhao et al. [80] is 353 K and the same for Liao and Roberts [81] is 298 K. On a similar note, Fig. 5 (b) shows the comparison of performance of mechanism A and B in predicting laminar burning velocity with the experimental data from Dirrenberger et al. [61] for 34.06% *iso*-octane/12.28% *n*-heptane/53.66% toluene (by mol) blend and Liao and Roberts [81] for 87% *iso*-octane/5.47% *n*-heptane/7.53% toluene (by mol) blend in air at atmospheric pressure. It is evident from the figure that the agreement between the mechanism predictions and the experimental results are quite good in the lean and near stoichiometric region. However, a maximum deviation between the predicted and experimental data of around 16% has been observed at $\varphi =$ 1.3 for mechanism B at 358 K. Moreover, around 14% difference between the experimental data and the model prediction has been observed at $\varphi = 1.5$ for mechanism A at 298 K.

The experimental data [82] on the laminar burning velocity of TPRF-air mixtures at higher pressures (i.e. 2 atm and 6 atm) is used in Fig. 5 (c) for the purpose of validation. The TPRF composition is same as the one used in Fig. B2 (a). It can be seen from Fig. 5 (c) that both the proposed mechanisms predict the laminar burning velocity of the TPRF-air mixture quite accurately. The laminar burning velocity of the biofuel components DMF and DME at atmospheric pressure and 300 K unburnt gas temperature is validated in Fig. 5 (d). The experimental data are taken from Somers et al. [26] for DMF and Wang et al. [83] for DME in air. It is evident from the figure that both mechanism A and B predict the laminar burning velocity of DMF-air mixtures well within the uncertainty range of the experimental data for $0.65 \leq \varphi \leq 1.55$. For DME, both mechanism A and B predict the laminar burning velocity within ± 10% range of the experimental data for $0.7 \leq \varphi \leq 1.2$. However, there is noticeable overprediction by both the proposed mechanisms for the rich DME-air mixtures at $\varphi > 1.2$. It can be seen from Figs. 4 and 5 that the overall performance of mechanism A and B is quite acceptable for the reproduction of experimental data from 1-D flames involving TPRF components, DMF, and DME. Although some deviations from experimental values of laminar burning velocity have been observed mostly in rich flames, it may be noted that modern SI engines seldom operate at such conditions.

The final part of the validation process includes the focus on the soot related chemistry of mechanism A and B. It may be mentioned in this regard that the polycyclic aromatic hydrocarbons (PAHs) generated in flames are considered as soot precursors [84] along with smaller species like propargyl (C_3H_3), vinylacetylene (C_4H_4), and 1,3-butadiene (C_4H_6). These smaller species participate in the formation of the first benzene ring and its further development into the PAH structure [84,85]. The

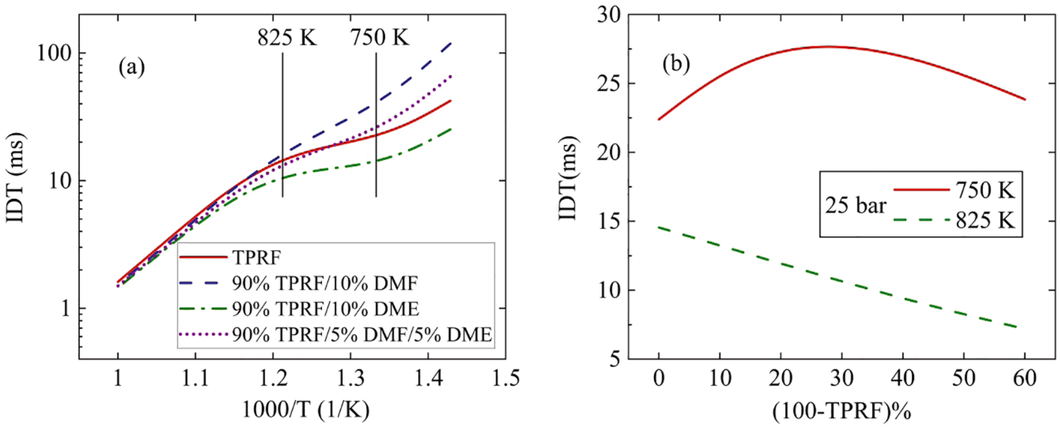

Fig. 6. (a) Variation of ignition delay time of TPRF-air mixture with different proportions of DMF and DME in fuel. (b) Variation of ignition delay time of stoichiometric TPRF-air mixture with biofuel (50% DMF/50% DME by mole) blending at 750 K and 825 K. The simulations have been performed with mechanism A at 25 bar for stoichiometric fuel–air mixtures. The TPRF composition is 34.06% *iso*-octane/12.28% *n*-heptane/53.66% toluene (by mol).

ability of mechanism A and B in predicting the gaseous soot precursors are shown in Fig. B3 (a-d) in Appendix B. The experimental data is taken from Dmitriev et al. [79] for the same flame depicted in Fig. 4 (b). It can be seen from the figure that both the mechanisms provide qualitative prediction quite accurately. Moreover, mechanism B performs better than mechanism A in predicting the benzene (C_6H_6) mole fraction in the flame.

It may be noted here that unlike mechanism A, mechanism B contains a comprehensive PAH mechanism. Therefore, mechanism B has been adopted in the next section for predicting soot precursors in 1-D flames involving TPRF/DMF/DME blends. As a basis for such an analysis, the relevant sub-mechanisms of C_2H_2, C_4H_6, and PAHs (naphthalene, phenanthrene, and pyrene) in mechanism B are validated and shown in Figs. B4 and B5 (Appendix B). Fig. B4 shows that mechanism B predicts the recent experimental data [86,87] on laminar burning velocity for acetylene (C_2H_2) and 1,3-butadiene (C_4H_6) quite accurately. Fig. B5 (a-c) shows that the experimental data on mole fractions of naphthalene, phenanthrene, and pyrene [88] are quite accurately predicted by mechanism B for premixed flat flames involving *n*-heptane/O_2/Ar mixture at $\varphi = 2.1$ and atmospheric pressure. Similar to Figs. 4 and B3, only the species conservation equations have been solved (using mechanism B) for Fig. B5 (a-c). It may be noted here that mechanism B performs particularly well in predicting the PAH mole fractions at the exit point of the flame where the temperature is high. On a similar note, the naphthalene mole fractions during the pyrolysis of TPRF mixture (8% *iso*-octane/14.5% n-heptane/77.5% toluene) are also predicted within the experimental uncertainty limit [89] in Fig. B5 (d) at high temperatures. These simulations have been performed in a perfectly stirred reactor with 76 cm^3 volume, 1 s residence time, and 0.25 % fuel concentration in N_2. The details of the mixture compositions (moles) used for validation in this section are given in Table A1 (Appendix A).

4. Results and discussion

After the validation of mechanism A and B, they have been used to predict the effects of DMF and DME blending on important combustion characteristics of stoichiometric TPRF-air mixtures in this section. First, mechanism A has been used to assess the changes in IDT of TPRF-air mixture due to DMF and DME blending in section 4.1. This choice is motivated by the fact that mechanism A contains a detailed low temperature chemistry and therefore performs better in the low and intermediate temperature range (Fig. 3). However, mechanism B is quite concise and therefore, requires lower computational resource. Hence, 1-D premixed flames of TPRF, and its blends with DMF and DME are analyzed using mechanism B in sections 4.2, 4.3, and 4.4.

4.1. *Effects of DMF and DME blending on ignition delay time of TPRF*

In this section, the effects of blending DMF and DME to TPRF IDT is analyzed from the perspective of modern gasoline engine application. It has been shown by Singh et al. [90] that the ignition delay times at 25 bar pressure and temperatures of 750 K and 825 K correlate quite accurately with the RON and MON of a wide range of gasoline surrogates respectively. Both these conditions fall in the low to intermediate temperature range or the NTC region [91] of IDTs for TPRF mixtures. As seen from Fig. 3, DME exhibits distinct NTC chemistry while DMF does not show the behavior [28]. Therefore, Fig. 6 (a) shows the variation of IDTs of TPRF, 90% TPRF/10% DMF, 90% TPRF/10% DME, and 90% TPRF/5% DMF/5% DME blends at 25 bar and temperature range of 700–1000 K.

It is evident from Fig. 6 (a) that the ignition inhibiting effect of DMF is stronger than the promoting effect of DME for $T \leq 750$ K. At 750 K, 10 % DMF blending causes the IDT to increase by 80% with respect to TPRF-air mixture. On the other hand, 10 % DME blending causes the IDT to shorten by only 37% with respect to TPRF-air mixture at 750 K. Moreover, the ability of DMF to suppress ignition grows more in the low temperature region. Due to this stronger effect of DMF addition, the IDT is 15% higher than TPRF for the 90% TPRF/5% DMF/5% DME blend at 750 K. On the other hand, the ignition promoting effect of DME is stronger than the suppressing effect of DMF at 825 K. While 10% DME addition causes 27 % decrease in the IDT of TPRF-air mixture, there is only around 10% gain in IDT when 10% DMF is blended (Fig. 6 (a)). As a result of the stronger ignition promoting effect of DME addition, the IDT is 9% lower than TPRF for the 90% TPRF/5% DMF/5% DME blend at 825 K.

For investigating the effect of DMF and DME blending further, the variation of IDT of TPRF-air mixture with different amounts of equimolar DMF/DME mixture blending is shown in Fig. 6 (b) at 750 K and 825 K. At 750 K, the IDT monotonously increases up to 20% blending point due to the dominance of DMF chemistry that suppresses the NTC behavior of TPRF and DME. However, the DME chemistry shows more influence beyond this point, thereby flattening the IDT growth. The

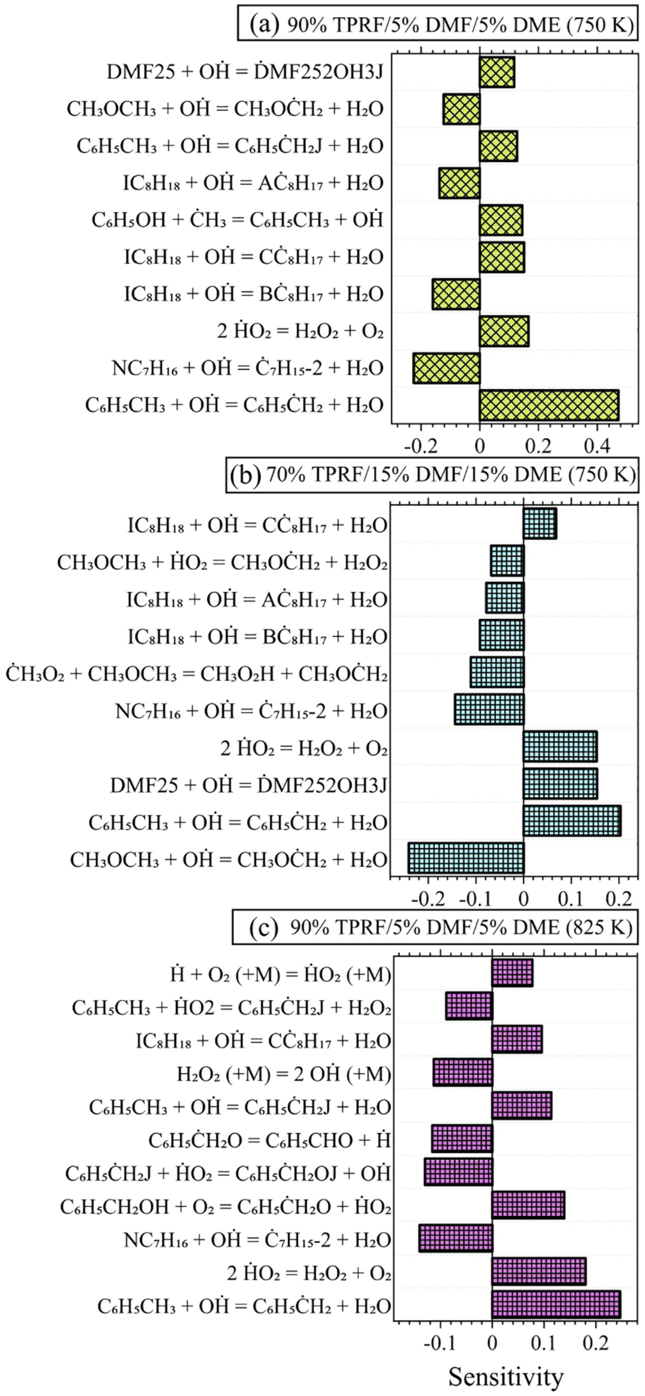

Fig. 7. Brute force sensitivity analysis of ignition delay time at (a) 750 K for 90% TPRF/5% DMF/5% DME, (b) 750 K for 70% TPRF/15% DMF/15% DME, and (c) 825 K for 90% TPRF/5% DMF/5% DME-air mixture at stoichiometric condition and 25 bar.

dominance of DME causes the IDT to decrease beyond 30% blending point. On the other hand, the IDT of TPRF decreases monotonously with the equimolar blending of DMF and DME at 825 K. Around 50 % decrease in the IDT has been observed in Fig. 6 (b) for 40% TPRF/30% DMF/30% DME blend compared to TPRF at 825 K.

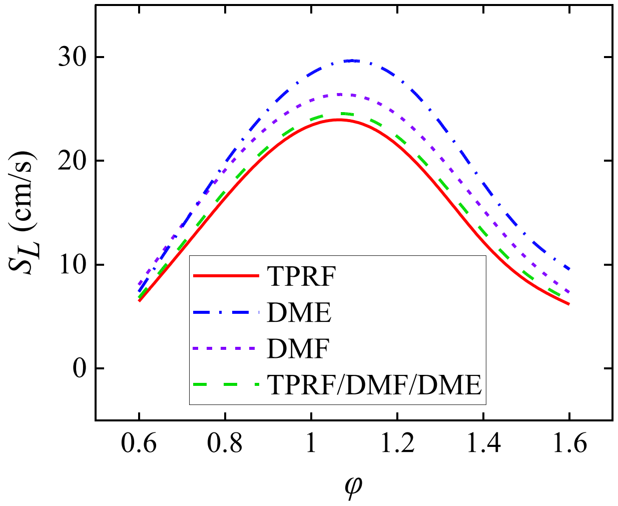

Fig. 8. Laminar burning velocity of TPRF, DME, DMF, and 50% TPRF/25% DMF/25% DME-air mixtures at 353 K unburnt gas temperature and 10 atm pressure. The simulations have been performed with mechanism B.

As mentioned earlier, the changes in IDTs due the DMF and DME blending to TPRF are reflected in the RON and MON as well. In the present work, correlations from Naser et al. [5] and Singh et al. [90] have been adopted to estimate the RON and MON of TPRF/DMF/DME blends from Fig 6 (b). These estimated values of RON, MON, and OS are shown in Fig. B6 (Appendix B). As seen from the figure, the estimated RON values are around 103 and 98 with the correlations from Naser et al. [5] and Singh et al. [90] respectively. On the other hand, the correlation from Naser et al. [5] predicts a monotonous decrease of MON—in the range 91 to 84—for the TPRF/DMF/DME blends. The Singh et al. [90] correlation estimates a MON value of around 91. Therefore, these estimates suggest either an increasing OS [5] (Fig. B6) or a constant value of 7 [90] if the equimolar DMF/DME mixture proportion is increased in TPRF. The former OS trend is also in line with the observation from Fig 6 (b) where the differences in IDT values at RON and MON relevant conditions increase with increase in equimolar DME/DMF mole fraction in the TPRF mixture. This way, the tri-fuel blend of TPRF/DMF/DME is expected to provide higher efficiency for the boosted SI engines [12,92].

To identify the influence of different chemical reactions on the ignition inhibiting (and promoting) effect of DMF (and DME) observed in Fig. 6 (b), brute force sensitivity analysis has been performed for stoichiometric fuel–air mixtures at (a) 750 K for 90% TPRF/5% DMF/5% DME, (b) 750 K for 70% TPRF/15% DMF/15% DME, and (c) 825 K for 90% TPRF/5% DMF/5% DME blends at 25 bar. The sensitive reactions are shown in Fig. 7 (a-c). The ‘Sensitivity’ of a reaction ‘*i*’ is defined as (IDT (2k_i)-IDT (k_i))/ IDT (k_i), where ‘k_i’ is the specific forward reaction rate, IDT (k_i) and IDT (2k_i) are the original IDT and the changed IDT with doubled specific forward reaction rate respectively. According to this definition, a positive sensitivity coefficient denotes a reaction that increases IDT and vice versa.

For the 90% TPRF/5% DMF/5% DME case in Fig. 7 (a), the H abstraction from toluene through $C_6H_5CH_3 + OH = C_6H_5\dot{C}H_2 + H_2O$ is the most influential reaction towards inhibiting ignition. The increase in IDT is further aided by the phenol (C_6H_5OH) breakup reaction $C_6H_5OH + \dot{C}H_3 = C_6H_5CH_3 + OH$. This C_6H_5OH decomposition reaction shows positive sensitivity because of the production of $C_6H_5CH_3$ molecules that increase ignition delay time primarily through the chain propagating

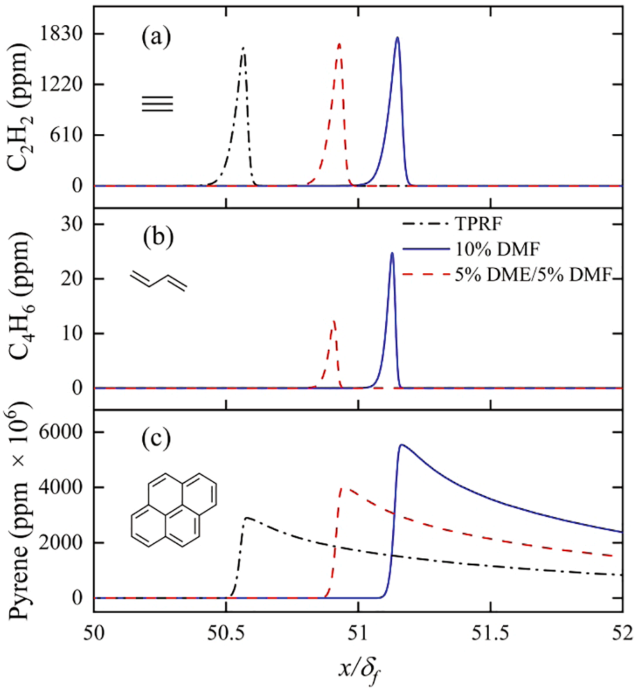

Fig. 9. Variation of gaseous soot precursors (a) acetylene (C_2H_2), (b) 1,3-butadiene (C_4H_6), and (c) pyrene across the normalized computational domain for stoichiometric TPRF, 90% TPRF/5% DME/5% DMF, and 90% TPRF/10% DMF blends in air at 10 bar pressure and unburnt gas temperature of 353 K. Mechanism B has been adopted for computation.

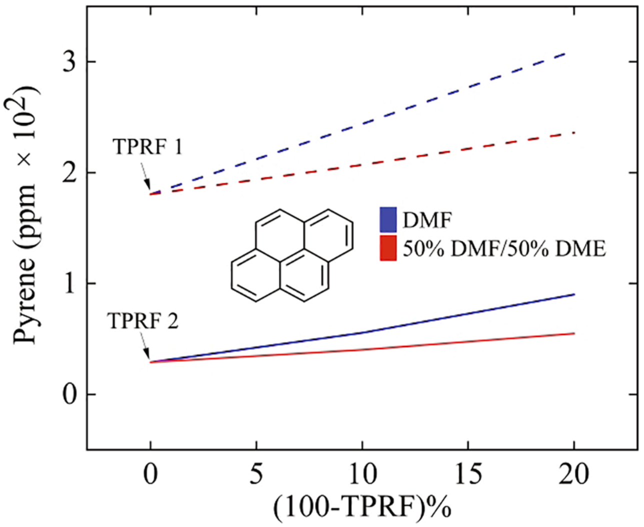

Fig. 10. Variation of maximum pyrene mole fraction in stoichiometric laminar premixed flames with biofuel blend ratio in two TPRF blends (1: 34.06% *iso*-octane /12.28% n-heptane /53.66% toluene and 2: 67% *iso*-octane /5% n-heptane /28% toluene by mol) at 10 bar pressure and unburnt gas temperature of 353 K. Mechanism B has been used and the biofuel composition is 100% DMF and 50% DMF/50% DME.

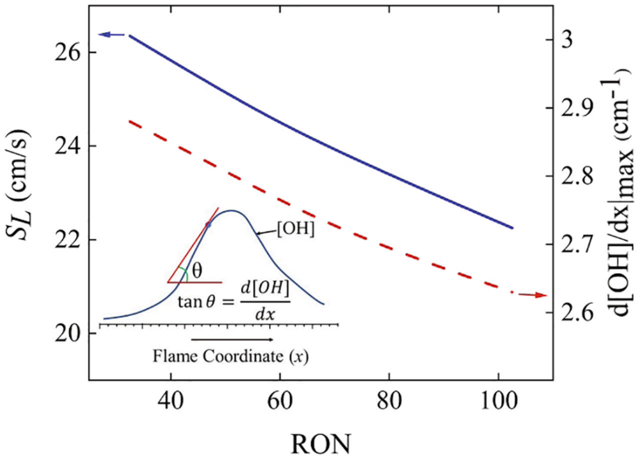

Fig. 11. Variation of laminar burning velocity and maximum slope of $O\dot{H}$ mole fraction trajectory in the stoichiometric 1-D flame involving 80% PRF/20% Toluene blends in air. Mechanism B has been adopted for simulation at 10 atm unburnt gas pressure and 353 K temperature.

reaction $C_6H_5CH_3 + OH = C_6H_5\dot{C}H_2 + H_2O$. The prevalence of the intermediate temperature chemistry is also evident in Fig. 7 (a) with the positive sensitivity of (a) the peroxide formation reaction $2HO_2 = H_2O_2 + O_2$ and (b) the OH addition to the furan ring to form 2,5-dimethyl-2-hydroxyl-2,3-dihydrofuran-3-yl radical (DMF252OH3J) [29]. On the other hand, the ignition is mainly promoted by the H abstraction reactions of *n*-heptane, *iso*-octane, and DME for stoichiometric 90% TPRF/5% DMF/5% DME-air mixture in Fig. 7 (a). The ignition promoting effect of the DME decomposition reaction $CH_3OCH_3 + OH = CH_3O\dot{C}H_2 + H_2O$ is augmented for the 70% TPRF/15% DMF/15% DME blend in Fig. 7 (b). The higher influence of DME chemistry towards the reduction of IDT is clear from the presence of the H abstraction reactions $\dot{C}H_3O_2 + CH_3OCH_3 = CH_3O_2H + CH_3O\dot{C}H_2$ and $CH_3OCH_3 + H\dot{O}_2 = CH_3O\dot{C}H_2 + H_2O_2$.

It can be observed from Fig. 7 (a) and (b) that unlike the formation *iso*-octyl isomers $A\dot{C}_8H_{17}$ and $B\dot{C}_8H_{17}$, the formation of $C\dot{C}_8H_{17}$ inhibits ignition. Similar observations have been reported earlier by Sarathy et al. [93] for different gasoline surrogates as well. The ignition suppressing effect of $IC_8H_{18} + OH = C\dot{C}_8H_{17} + H_2O$ is also evident in Fig. 7 (c) for 90% TPRF/5% DMF/5% DME blend at 825 K. The main cause behind this fact is (a) unlike $A\dot{C}_8H_{17}$ and $B\dot{C}_8H_{17}$, the *β*-scission of $C\dot{C}_8H_{17}$ does not produce methyl ($\dot{C}H_3$) radicals and (b) $C\dot{C}_8H_{17}$ reacts with O_2 to produce hydroperoxy radicals ($H\dot{O}_2$) that have low reactivity. The $\dot{C}H_3$ radicals can promote reactivity by abstracting H radicals from *iso*-octane molecule.

The sensitivity analysis shown in Fig. 7 (a) and (b) suggest that the competition between the DMF and DME chemistries determine the increase or decrease of IDT at 750 K. However, such a competition is not seen at 825 K in Fig. 7 (c) for 90% TPRF/5% DMF/5% DME blend. Rather, the influence of high temperature chemistry is evident here as H_2O_2—formed through $2HO_2 = H_2O_2 + O_2$—breaks to form OH radicals [43] and increases reactivity. Moreover, the toluene decomposition reaction $C_6H_5CH_3 + OH = C_6H_5\dot{C}H_2 + H_2O$ suppresses ignition to the largest extent at 825 K in Fig. 7 (c). Therefore, it can be inferred from the sensitivity analysis in Fig. 7 (c) that the monotonously decreasing trend of IDT in Fig. 6 (b) at 825 K is caused by the dominance of the high temperature chemistry of TPRF.

The flattening of the IDT variation at 30% blending point observed in Fig. 6 (b) indicates that the 80% TPRF/10% DMF/10% DME blend is optimum from the perspective of gain in ignition resistance at 750 K and 25 bar. Below the 20% blending ratio, the DMF combustion chemistry influences the ignition phenomenon and therefore, IDT increases monotonously. Between 20 and 30% blending ratio, the IDT growth is flat due to the dominance of DME chemistry. Moreover, when the equimolar mixture of DMF/DME exceeds the 30% blending proportion mark in TPRF, the IDT decreases due to the increased influence of DME.

4.2. Effect of DMF and DME blending on the laminar burning velocity of TPRF

Similar to the IDT, laminar burning velocity is an important fundamental combustion parameter for fuel–air mixtures as well. It has strong influence on the reactivity, diffusivity, flame stability, and turbulent flame propagation inside the engine cylinder [94]. Therefore, it is important that the change in laminar burning velocity is minimized when DMF and DME is blended to gasoline. Fig. 8 shows the variation of the laminar burning velocity of TPRF, DME, DMF, and 50% TPRF/25% DMF/25% DME-air mixture with equivalence ratio. The TPRF surrogate composition corresponding to FACE C gasoline (34.06% *iso*-octane/12.28% *n*-heptane/53.66% toluene (by mol)) has been used. The unburnt gas temperature and pressure is 353 K and 10 atm respectively. This high-pressure condition is closer to the in-cylinder condition in SI engines. Moreover, it may be noted that the laminar burning velocity is strongly correlated in the unburnt pressure–temperature space [71].

It can be observed from Fig. 8 that the laminar burning velocity of DME and DMF is around 21% and 10% higher than the TPRF-air mixture at stoichiometric condition respectively. However, the increase in laminar burning velocity for 50% TPRF/25% DMF/25% DME-air mixture is only 2% compared to the TPRF-air case at $\varphi = 1$. In fact, the increase is less than 10% for 50% TPRF/25% DMF/25% DME-air mixture compared to the TPRF-air case for all equivalence ratios. The maximum amount of deviation (≈9%) has been observed at $\varphi = 1.4$ for 50% TPRF/25% DMF/25% DME-air mixture compared to the TPRF-air case. Such a minimal deviation in laminar burning velocity is also beneficial from the SI engine design perspective.

4.3. Soot emission analysis from DMF and DME blended TPRF flames

In the next step of the present study, soot emission from TPRF/DMF/DME blend is analyzed in the premixed 1-D flame context. Although many studies have highlighted the suitability of DMF as a gasoline blend component, the molecular structure of DMF (containing $C = C$ double bond and heteroaromatic ring) has an inclination towards augmenting soot emission from flames [10,31,95]. On the other hand, Ji et al. [16] have shown that DME can successfully be blended with gasoline to reduce soot emissions from SI engine. The absence of C–C bonds, high oxygen content (34.8% by mass), and second lowest carbon-to-hydrogen ratio (C/H) (after methane) make the combustion of DME almost soot free.

The effects of adding DME (to the TPRF/DMF blend) on the soot precursor mole fractions in the 1-D laminar burner-stabilized flame are discussed in the following part. Initially, the variations of C_2H_2, C_4H_6, and pyrene across the 1-D flames for TPRF, 90% TPRF/5% DME/5% DMF, and 90% TPRF/10% DMF blends in air (at 10 bar pressure and unburnt gas temperature of 353 K) are analyzed. The TPRF composition is 67% *iso*-octane /5% n-heptane /28% toluene by mol (by mol). The choice of this TPRF composition is motivated by the facts (a) it has high ON rating (RON = 98) [5] like modern gasolines and (b) the aromatic content is in the realistic range [4]. It may be seen from Fig. 9 (a) that the addition of 10% DMF (by mole) to TPRF increases the maximum mole fraction of C_2H_2 slightly with respect to the TPRF-air mixture. On the other hand, the maximum mole fraction of C_2H_2 for the 90% TPRF/5% DME/5% DMF blend is lower than the 10% DMF case. The abscissa in Fig. 9 has been normalized with the flame thickness $\delta_f = (T_{ad} - T_u)/(\nabla T)_{\max}$, where T_{ad} is the adiabatic flame temperature, T_u is the unburnt gas temperature and $(\nabla T)_{\max}$ is the maximum temperature gradient in the flame [96].

It has been observed in the present study that the TPRF-air flame generated negligible amount of C_4H_6. However, for the 10% DMF case, the maximum mole fraction is around 25 ppm (Fig. 9 (b)). This increase may be attributed to the H abstraction reaction $DMF + H = C_4H_6 + CH_3CO$ where the initial breakup of the fuel molecule contributes to C_4H_6 formation. There is around 50% reduction in the peak C_4H_6 value for the 90% TPRF/5% DME/5% DMF case in comparison to the 90% TPRF/10% DMF blend. One of the important routes towards the first benzene ring formation (in the PAH generation path) is the 1,3-butadiene $\xrightarrow{+C_2H_2}$ 1,3-butadien-2-yl (i-C_4H_5)/ normal butadienyl (n-C_4H_5) $\Rightarrow^{+C_2H_2}$fulvene $\xrightarrow{+\dot{H}}$ benzene [97,98]. Along with being a key species in this route, C_2H_2 also contributes in the growth of the benzene ring through hydrogen abstraction C_2H_2 addition (HACA) mechanism [84]. As a combination of these facts, it may be seen in Fig. 9 (c) that the peak value of pyrene mole fraction increases by 90% when 10% DMF is blended to TPRF. The same increase is only 33% for the 90% TPRF/5% DME/5% DMF blend.

Finally, the variation of maximum pyrene mole fraction with DMF and 50% DMF/50% DME blend ratio in TPRF is compared in Fig. 10 at 10 bar pressure and unburnt gas temperature of 353 K. Two different TPRF blends have been adopted in the figure to show the effect of TPRF composition on maximum pyrene mole fraction. It may be observed from the figure that DMF blending in TPRF causes steep rise in the pyrene mole fraction for both the TPRF blends. TPRF 1 produces more pyrene due to its higher toluene content. The rate of increase of peak pyrene mole fraction is lower for the equimolar DMF/ DME case. It has been observed in the present work that 20% blend of 50% DMF/50% DME mixture in TPRF 2 reduces the peak pyrene mole fraction by around 40% in comparison to the 20% DMF case. Therefore, it can be summarized from Figs. 9 and 10 that the addition of DME causes significant reduction in soot precursors in TPRF/DMF-air flames due to its ability to burn soot free.

It is evident from the above analysis that an equimolar mixture of DMF/DME is better than only DMF as a blending component for gasoline from the perspective of soot emissions. As seen from Fig. 9, the increase in peak pyrene mole fraction is only around 1.36 times the value of the TPRF-air case when the 5% DMF and 5% DME is blended simultaneously. Whereas, the same increase is around 100% when 10% DMF is blended to TPRF. Therefore, a combination of the facts presented in section 4.1 and 4.3 suggest that (a) the simultaneous blending of DMF and DME in TPRF is advantageous for RON and OS but (b) the blending proportion of DMF and DME in TPRF is limited by soot generation.

4.4. Correlation of RON with 1-D flame structure of TPRF-air mixture

Modern SI engines require high octane gasolines for efficient operation [92]. According to a recent study by Szybist et al. [12], RON has the largest impact on the SI engine efficiency. Faster laminar burning velocity results in quicker compression of the end-gas by the propagating flame front [91]. This way, the end-gas gets less time for heat loss into the surroundings and the chances for pre-ignition increases [99]. In this context, Fagundez et al. [100] have recently shown that a decreased laminar burning velocity results in a reduced risk for knock onset. Therefore, laminar burning velocities of stoichiometric TPRF-air mixtures have been plotted against the corresponding RON values in Fig. 11 at 10 atm pressure and 353 K unburnt gas temperature. In the TPRF mixtures used for Fig. 11, the toluene liquid volume fraction is kept constant at 20% to contain the aromatic content near realistic gasoline range. The PRF composition has been varied for changing the RON values. The RON values for the TPRFs have been calculated from the blending rule proposed by Kalghatgi et al. [101]. This blending rule is able to predict the experimental values of RONs for TPRFs in literature with high R^2 (=0.9998) value [101] for RON < 100. Therefore, Naser et al. [5] have also used it for calculating RON and MON values of a wide variety of TPRF mixtures.

The laminar burning velocity is seen to be varying reciprocally with the RONs for stoichiometric 80% PRF/20% toluene-air mixtures in Fig. 11. Quantitatively, the laminar burning velocity increases by 18% when the RON decreases from 102.5 to 32.5. The increased reactivity of the TPRF mixtures inferred from the increased laminar burning velocity and consequently decreased RON stems from the augmented active radical concentration in the flame. Moreover, such an increase in the active radical concentration may be attributed to the increase in the linear paraffin (n-heptane) content. The linear structure of n-heptane breaks more readily to form active radicals in comparison to the branched structure of *iso*-octane [42,71]. The forward reaction rate of $\dot{H}$ radical producing reactions $CO + OH = CO_2 + \dot{H}$ and $HCO + M = \dot{H} + CO + M$ have positive impact on the laminar burning velocity [102] as well.

The $\dot{H}$ radicals increase the laminar burning velocity due to their high diffusivity and ability to break alkane structures into primary alkyl radicals. Additionally, the $\dot{H}$ radicals generated in the above-mentioned reaction steps finally participate in the chain branching reaction $\dot{H}+O_2 = \dot{O}+O\dot{H}$ to increase the reactivity in the flame [70,102]. Therefore, it may be seen from Fig. 11 that the maximum slope of the $O\dot{H}$ radical mole fraction in the computational domain shows similar trend with RON as compared to the laminar burning velocity. It is worth mentioning in this context that the IDT is also commonly measured from the temporal variation of the OH radicals [75]. Therefore, the proportionality of the maximum slope of the $O\dot{H}$ radical mole fraction with RON in Fig. 11 is in line with the recent studies where the changes in reactivity have been expressed through IDT and correlated with RON [5,90,103]. It can be mentioned here that similar relationships have been observed between laminar burning velocity, $\left.\frac{d[O\dot{H}]}{dx}\right|_{max}$, and RON for other TPRF blends as well. However, it may be noted here that the experimental data for RON does not exist in literature for TPRF/DME/DMF blends. Therefore, the extension of the analysis shown in Fig. 11 for this tri-fuel blend has been kept outside of the scope of the present work.

5. Conclusions

In the present work, the effects of blending DMF and DME on the 0-D and 1-D combustion of toluene primary reference fuels have been studied numerically. Two chemical kinetic mechanisms (mechanism A and B) have been formulated for the analysis. Experimental data from literature have been used for the validation of the proposed mechanisms at wide range of parametric conditions. The main findings of present work can be summarized as follows:

1. The validation study suggests that,
   a) Mechanism A (504 species and 4212 reactions) predicts the ignition delay time more accurately than mechanism B (153 Species and 740 Reactions)
   b) Mechanism B is more suitable for the simulation of laminar burning velocity of fuel blends involving *iso*-octane, *n*-heptane, toluene, DMF and DME.
   c) Mechanism B can successfully predict the concentrations of gaseous soot precursors generated in 1-D flames.
2. There is significant variation in the intermediate-temperature ignition delay time when DMF and DME are blended to TPRF. The salient points about such variations are,
   a) DME decreases the ignition delay time of stoichiometric TPRF-air mixture due to the presence of NTC chemistry. On the contrary, DMF does not exhibit NTC behavior and therefore its blending with TPRF prohibits ignition.
   b) At 750 K and 25 bar, the ignition promoting effect of DME is significantly weaker than the inhibiting effect of DMF when 10% DMF or DME is blended with TPRF by mole. Therefore, an increase of 15% in ignition delay time of 90% TPRF/5% DMF/5% DME blend compared to TPRF-air mixture has been observed for $\varphi = 1$.
   c) The benefits of adding DMF (in increasing IDT) are neutralized for 70% TPRF/15% DMF/15% DME blend in air (at $\varphi = 1$, 750 K and 25 bar) due to the dominance of DME breakup pathways.
   d) The IDT of TPRF decreases monotonously with the blending of DMF and DME at 825 K and 25 bar.
3. There is minimal variation (around 4% at $\varphi = 1$) in the laminar burning velocity when DMF and DME are blended to TPRF in equimolar proportions at atmospheric pressure and 300 K unburnt gas temperature.
4. Due to the coupling between $\dot{H}$ and OH radicals through $\dot{H}+O_2 = \dot{O}+O\dot{H}$, both laminar burning velocity and the maximum slope of the OH radical mole fraction in the 1-D computational domain $\left(\left.\frac{d[O\dot{H}]}{dx}\right|_{max}\right)$ show linear reciprocal variation with RON for stoichiometric TPRF-air mixtures.
5. The peak pyrene (4 ring PAH) mole fraction in stoichiometric 1-D flame increases by 90% when 10% DMF is blended into TPRF. However, the presence of DME helps to mitigate PAH generation to a great extent.

The present chemical kinetic study of TPRF/DMF/DME blend indicates that the presence of DMF in gasoline can enhance the knock resistance to a great extent for modern boosted gasoline engines. The simultaneous presence of DMF and DME also has the potential to increase the OS of gasoline. On the other hand, the presence of DME helps in suppressing additional soot generation due to DMF blending. Therefore, simultaneous DMF and DME blending (in gasoline) in low concentrations (~20%) complement each other in providing efficient SI engine operation with low soot emission. Future scope of work includes the implementation of the skeletal mechanism (mechanism B) for further investigation of the above-mentioned facts with 1-D and 3-D CFD analysis of SI engine combustion.

CRediT authorship contribution statement

Atmadeep Bhattacharya: Conceptualization, Methodology, Software, Validation, Visualization, Writing - original draft, Formal analysis. **Ali Shahanaghi:** Software, Writing - review & editing. **Ossi Kaario:** Supervision, Writing - review & editing. **Ville Vuorinen:** Supervision, Funding acquisition, Writing - review & editing. **Rupali Tripathi:** Conceptualization, Writing - review & editing. **Teemu Sarjovaara:** Conceptualization, Methodology.

Declaration of Competing Interest

The authors declare that they have no known competing financial interests or personal relationships that could have appeared to influence the work reported in this paper.

Acknowledgments

This work was funded by Neste Oy. The authors acknowledge the computational resources provided by the Aalto Science-IT project.

Appendix A

Table A1
List of experimental data used for validation.

Figure	Composition (mole)	Pressure	Temperature	φ	Reference ST	RCM
			Ignition Delay Time			
3 (a)	*iso*-octane-air	10 bar	600–1660 K	1	[69]	[68]
3 (b)	PRF 70-air	10 bar	925–1240 K	1	[73]	
		20 bar	695–1170 K	1		
Inset	1.34% n-heptane/14.89% O_2/83.77% Ar	9 bar	615–885 K	1		[74]
3 (c)	36.5% *iso*-octane/35% n-heptane/28.5% toluene-air	20 bar	640–1180 K	1	[75]	[75]
		40 bar	625–1111 K	1	[75]	[75]
3 (d)	1.82% toluene/1.31% DME/20.34% O_2/76.53% diluent*	20 bar	650–1330 K	1	[76]	[76]
	0.29% n-heptane/0.29% DME/4.08% O_2/95.34% Ar	10 bar	1185–1355 K	1	[77]	
3 (e)	2.73% DMF/20.43% O_2/76.84% Ar	5 bar	1130–1390 K	1	[53]	
	0.25% DMF/1.875% O_2/97.875% Ar	1 bar	1430–1765 K	1	[22]	
3 (f)	1.05% *iso*-octane/1.05% DMF/20.57% O_2/77.33% Ar	12 bar	1080–1290 K	1	[53]	
	0.222% n-heptane/0.222% DMF/4.108% O_2/95.448% Ar	10 bar	1175–1600 K	1	[78]	
B1	PRF 80-air	20 bar	710–1200 K	1	[73]	
		40 bar	710–1150 K	1	[73]	
B2 (a)	34.06% *iso*-octane /12.28% n-heptane /53.66% toluene-air	20 bar	875–1190 K	0.5	[8]	
B2 (b)	1.38% DMF/20.72% O_2/77.9% Ar	12 bar	1000–1280 K	0.5	[53]	
B2 (c)	0.92% toluene/0.68% DME/20.66% O_2/77.74% diluent#	20 bar	1065–1375 K	0.5	[76]	
			1-D Species Profiles from Burner Stabilized Flame			
4 (a)	4.11% *iso*-octane/4.11% DME/41.77% O_2/50% Ar	40 mbar	Exp. Profile	1.53	[40]	
4 (b), B3	2.29% n-heptane /1.36% toluene/21.36% O_2/75% Ar	1 atm	Exp. Profile	1.75	[79]	
4 (c)	5.92% DMF/44.07% O_2/50% Ar	20 mbar	Exp. Profile	1.0	[24]	
B5 (a-c)	5.5% n-heptane/28.79% O_2/65.71% Ar	1 atm	Exp. Profile	2.1	[88]	
			Naphthalene Mole Fraction from Pyrolysis in Jet Stirred Reactor			
B5 (d)	8% *iso*-octane/14.5% n-heptane/77.5% toluene	1 atm	1030–1180 K	–	[89]	
			Laminar Burning Velocity			
5 (a)	63% *iso*-octane /17% n-heptane /20% toluene-air	1 atm	353 K	0.6–1.3	[80]	
	PRF 95-air	1 atm	298 K	0.8–1.3	[81]	
5 (b)	34.06% *iso*-octane /12.28% n-heptane /53.66% toluene-air	1 atm	358 K	0.6–1.5	[61]	
	87% *iso*-octane /5.47% n-heptane /7.53% toluene-air	1 atm	298 K	0.8–1.3	[81]	
5 (c)	34.06% *iso*-octane /12.28% n-heptane /53.66% toluene-air	2 atm	358 K	0.8–1.5	[82]	
		6 atm	358 K	0.8–1.2		
5 (d)	DMF-air	1 atm	300 K	0.6–1.6	[26]	
	DME-air	1 atm	300 K	0.6–1.6	[83]	
B4	Acetylene-air	1 atm	298 K	0.65–1.6	[86]	
	1,3-butadiene-air	1 atm	359 K	0.8–1.6	[87]	
			399 K	0.6–1.6		

*Diluent is composed of 30% N_2/70% Ar, 100% N_2, and 60% N_2/40% CO_2 for high, intermediate, and low temperature range respectively

Diluent is composed of 50% N_2/50% Ar

Appendix B

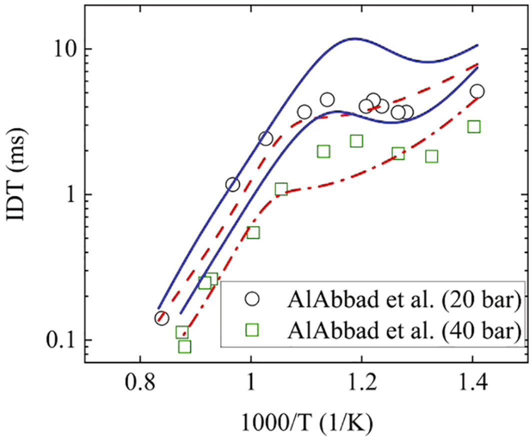

Fig. B1. Comparison of performance of mechanism A and mechanism B in predicting the experimental data on ignition delay time (IDT) from AlAbbad et al. [73] for stoichiometric PRF80-air mixture at 20 and 40 bar.

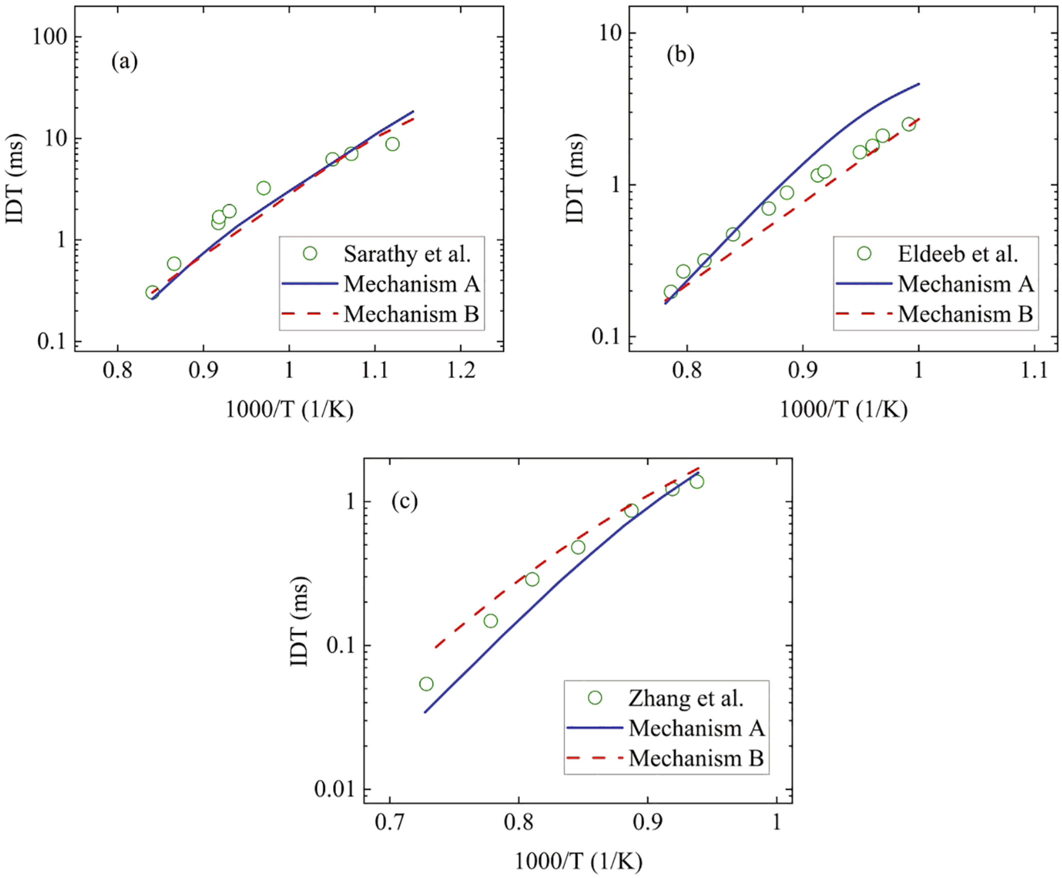

Fig. B2. Comparison of performance of mechanism A and mechanism B in predicting the experimental data on ignition delay time (IDT) from Sarathy et al. [8], Eldeeb et al. [53], and Zhang et al. [76] for $\varphi = 0.5$.

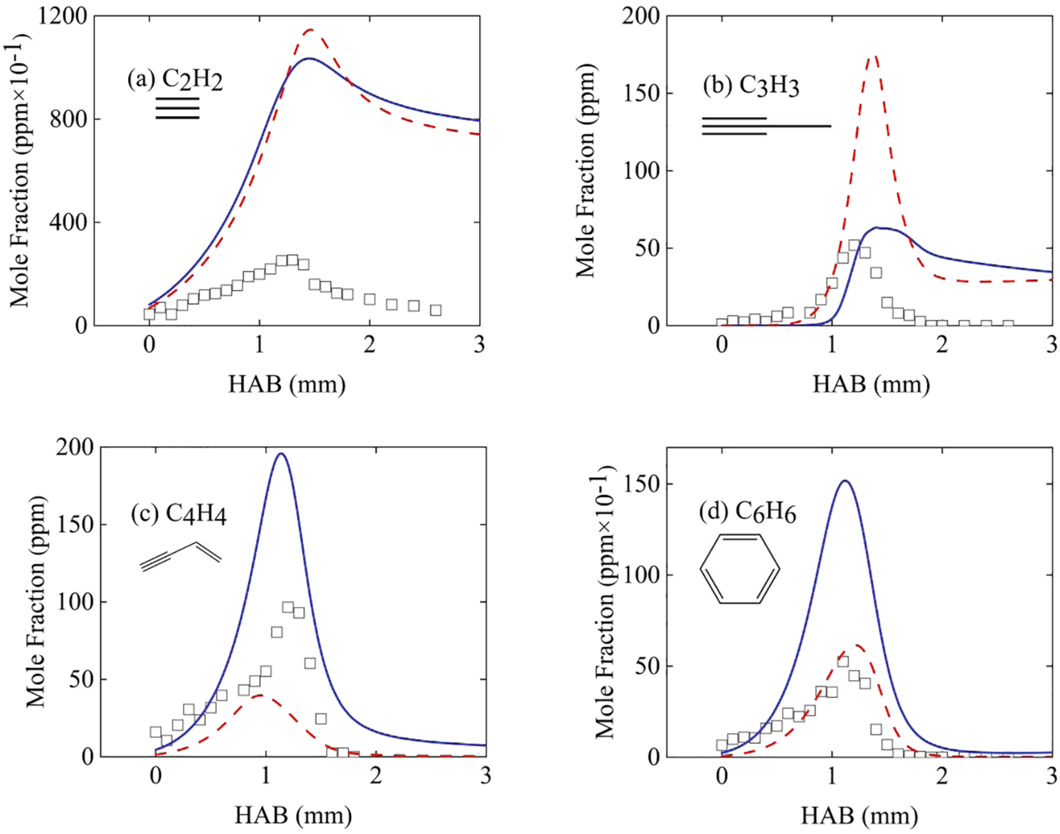

Fig. B3. Comparison of performance of mechanism A (bold lines) and mechanism B (dotted lines) in predicting the minor species profile distributions over the height above burner (HAB) for rich premixed 1-D flame ($\varphi = 1.75$) with experimental data (symbols) from Dmitriev et al. [79].

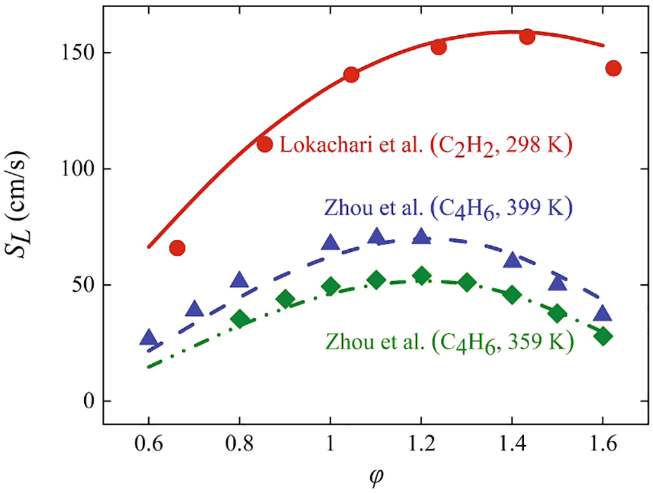

Fig. B4. Validation of laminar burning velocity predictions using mechanism B (lines) for acetylene (C_2H_2) with experimental data from Lokachari et al. [86] and 1,3-butadiene (C_4H_6) with experimental data from Zhou et al. [87]. All values are computed at atmospheric pressure.

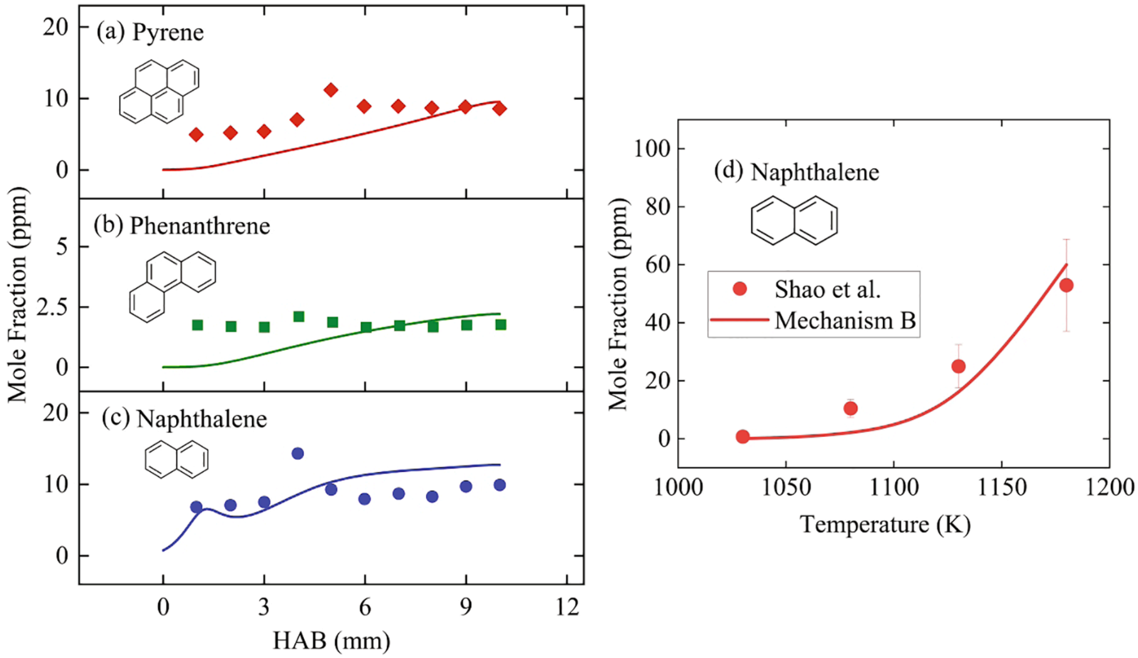

Fig. B5. Validation of the PAH mechanism in mechanism B against experimental data from (a-c) Inal et al. [88] for rich ($\varphi = 2.1$) flames involving n-heptane/O_2/Ar mixture and (d) Shao et al. [89] for pyrolysis of TPRF mixture in jet stirred reactor at atmospheric pressure.

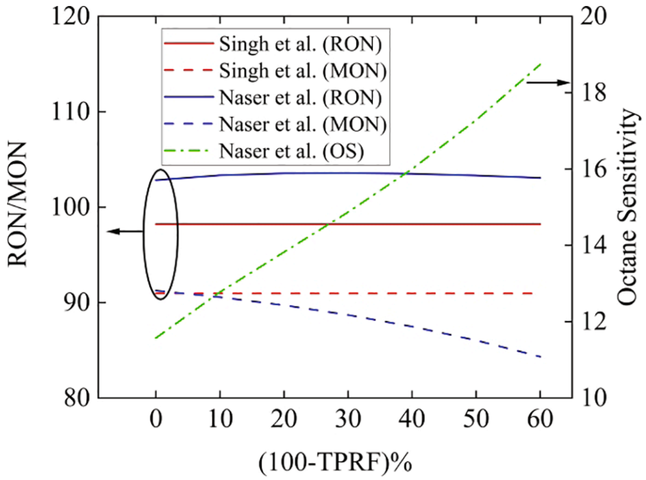

Fig. B6. Variation of octane numbers of TPRF-air mixture with different amounts of DMF and DME in equimolar proportions.

Appendix C. Supplementary data

Supplementary data to this article can be found online at https://doi.org/10.1016/j.fuel.2021.121401.

References

[1] Leach F, Kalghatgi G, Stone R, Miles P. The scope for improving the efficiency and environmental impact of internal combustion engines. Transp Eng 2020;1: 100005. https://doi.org/10.1016/j.treng.2020.100005.

[2] Kalghatgi G, Levinsky H, Colket M. Future transportation fuels. Prog Energy Combust Sci 2018;69:103–5. https://doi.org/10.1016/j.pecs.2018.06.003.

[3] W.J. Pitz N.P. Cernansky F.L. Dryer F.N. Egolfopoulos J.T. Farrell D.G. Friend et al. Development of an experimental database and chemical kinetic models for surrogate gasoline fuels SAE Tech. Pap. 2007 p. 2007–01–0175 10.4271/2007-01-0175.

[4] Sarathy SM, Farooq A, Kalghatgi GT. Recent progress in gasoline surrogate fuels. Prog Energy Combust Sci 2018;65:67–108. https://doi.org/10.1016/j.pecs.2017.09.004.

[5] Naser N, Sarathy SM, Chung SH. Estimating fuel octane numbers from homogeneous gas-phase ignition delay times. Combust Flame 2018;188:307–23. https://doi.org/10.1016/j.combustflame.2017.09.037.

[6] J.C.G. Andrae T. Kovács Evaluation of Adding an Olefin to Mixtures of Primary Reference Fuels and Toluene to Model the Oxidation of a Fully Blended Gasoline Energy and Fuels 30 9 2016 7721 7730 10.1021/acs.energyfuels.6b01193 10.1021/acs.energyfuels.6b01193.s001 10.1021/acs.energyfuels.6b01193.s002 10.1021/acs.energyfuels.6b01193.s003 10.1021/acs.energyfuels.6b01193.s004.

[7] Bianco A, Millo F, Piano A. Modelling of combustion and knock onset risk in a high-performance turbulent jet ignition engine. Transp Eng 2020;2:100037. https://doi.org/10.1016/j.treng.2020.100037.

[8] Sarathy SM, Kukkadapu G, Mehl M, Wang W, Javed T, Park S, et al. Ignition of alkane-rich FACE gasoline fuels and their surrogate mixtures. Proc Combust Inst 2015;35(1):249–57. https://doi.org/10.1016/j.proci.2014.05.122.

[9] Román-Leshkov Y, Barrett CJ, Liu ZY, Dumesic JA. Production of dimethylfuran for liquid fuels from biomass-derived carbohydrates. Nature 2007;447(7147): 982–5. https://doi.org/10.1038/nature05923.

[10] Qian Y, Zhu L, Wang Y, Lu X. Recent progress in the development of biofuel 2,5-dimethylfuran. Renew Sustain Energy Rev 2015;41:633–46. https://doi.org/10.1016/j.rser.2014.08.085.

[11] Rothamer DA, Jennings JH. Study of the knocking propensity of 2,5-dimethylfuran-gasoline and ethanol-gasoline blends. Fuel 2012;98:203–12. https://doi.org/10.1016/j.fuel.2012.03.049.

[12] Szybist JP, Busch S, McCormick RL, Pihl JA, Splitter DA, Ratcliff MA, et al. What fuel properties enable higher thermal efficiency in spark-ignited engines? Prog Energy Combust Sci 2021;82:100876. https://doi.org/10.1016/j.pecs.2020.100876.

[13] Shi L, Ji C, Wang S, Cong X, Su T, Shi C. Impacts of dimethyl ether enrichment and various injection strategies on combustion and emissions of direct injection gasoline engines in the lean-burn condition. Fuel 2019;254:115636. https://doi.org/10.1016/j.fuel.2019.115636.

[14] Shi L, Ji C, Wang S, Cong X, Su T, Wang Du. Combustion and emissions characteristics of a S.I. engine fueled with gasoline-DME blends under different spark timings. Fuel 2018;211:11–7. https://doi.org/10.1016/j.fuel.2017.09.019.

[15] Shi L, Ji C, Wang S, Su T, Cong X, Wang Du, et al. Effects of second injection timing on combustion characteristics of the spark ignition direct injection gasoline engines with dimethyl ether enrichment in the intake port. Energy 2019; 180:10–8. https://doi.org/10.1016/j.energy.2019.05.056.

[16] Ji C, Liang C, Wang S. Investigation on combustion and emissions of DME/gasoline mixtures in a spark-ignition engine. Fuel 2011;90(3):1133–8. https://doi.org/10.1016/j.fuel.2010.11.033.

[17] T. Lu C.K. Law Toward accommodating realistic fuel chemistry in large-scale computations Prog Energy Combust Sci 35 2 2009 192 215 10.1016/j.pecs.2008.10.002.

[18] Wu Y, Liu Y, Lu T. A linearized error propagation method for skeletal mechanism reduction. Combust Flame 2020;211:303–11. https://doi.org/10.1016/j.combustflame.2019.10.003.

[19] Bhattacharya A, Kaario O, Vuorinen V, Tripathi R, Sarjovaara T. Analysis of Gasoline Surrogate Combustion Chemistry with a Skeletal Mechanism. SAE Tech. Pap. 2020-01-2004, SAE International; 2020.

[20] Ranzi E, Frassoldati A, Grana R, Cuoci A, Faravelli T, Kelley AP, et al. Hierarchical and comparative kinetic modeling of laminar flame speeds of hydrocarbon and oxygenated fuels. Prog Energy Combust Sci 2012;38(4):468–501. https://doi.org/10.1016/j.pecs.2012.03.004.

[21] PEPIOTDESJARDINS P, PITSCH H. An efficient error-propagation-based reduction method for large chemical kinetic mechanisms. Combust Flame 2008; 154(1-2):67–81. https://doi.org/10.1016/j.combustflame.2007.10.020.

[22] Sirjean B, Fournet R, Glaude P-A, Battin-Leclerc F, Wang W, Oehlschlaeger MA. Shock tube and chemical kinetic modeling study of the oxidation of 2,5-dimethylfuran. J Phys Chem A 2013;117(7):1371–92. https://doi.org/10.1021/jp308901q.

[23] Liu D, Togbé C, Tran L-S, Felsmann D, Oßwald P, Nau P, et al. Combustion chemistry and flame structure of furan group biofuels using molecular-beam mass spectrometry and gas chromatography - Part I: Furan. Combust Flame 2014;161 (3):748–65. https://doi.org/10.1016/j.combustflame.2013.05.028.

[24] Togbé C, Tran L-S, Liu D, Felsmann D, Oßwald P, Glaude P-A, et al. Combustion chemistry and flame structure of furan group biofuels using molecular-beam mass spectrometry and gas chromatography - Part III: 2,5-Dimethylfuran. Combust Flame 2014;161(3):780–97. https://doi.org/10.1016/j.combustflame.2013.05.026.

[25] Tran L-S, Togbé C, Liu D, Felsmann D, Oßwald P, Glaude P-A, et al. Combustion chemistry and flame structure of furan group biofuels using molecular-beam mass spectrometry and gas chromatography - Part II: 2-Methylfuran. Combust Flame 2014;161(3):766–79. https://doi.org/10.1016/j.combustflame.2013.05.027.

[26] Somers KP, Simmie JM, Gillespie F, Conroy C, Black G, Metcalfe WK, et al. A comprehensive experimental and detailed chemical kinetic modelling study of 2,5-dimethylfuran pyrolysis and oxidation. Combust Flame 2013;160(11): 2291–318. https://doi.org/10.1016/j.combustflame.2013.06.007.

[27] Weber I, Friese P, Olzmann M. H-Atom-Forming Reaction Pathways in the Pyrolysis of Furan, 2-Methylfuran, and 2,5-Dimethylfuran: A Shock-Tube and Modeling Study. J Phys Chem A 2018;122(32):6500–8. https://doi.org/10.1021/acs.jpca.8b05346.

[28] Bhattacharya A, Datta A. Effects of blending 2,5-dimethylfuran on the laminar burning velocity and ignition delay time of isooctane/air mixture. Combust Theory Model 2019;23(1):105–26. https://doi.org/10.1080/13647830.2018.1492153.

[29] Liu X, Wang H, Wei L, Liu J, Reitz RD, Yao M. Development of a reduced toluene reference fuel (TRF)-2,5-dimethylfuran-polycyclic aromatic hydrocarbon (PAH) mechanism for engine applications. Combust Flame 2016;165:453–65. https://doi.org/10.1016/j.combustflame.2015.12.030.

[30] Tran LS, Wang Z, Carstensen HH, Hemken C, Battin-Leclerc F, Kohse-Höinghaus K. Comparative experimental and modeling study of the low- to moderate-temperature oxidation chemistry of 2,5-dimethylfuran, 2-methylfuran, and furan. Combust Flame 2017;181:251–69. https://doi.org/10.1016/j.combustflame.2017.03.030.

[31] Tran L-S, Sirjean B, Glaude P-A, Kohse-Höinghaus K, Battin-Leclerc F. Influence of substituted furans on the formation of Polycyclic Aromatic Hydrocarbons in flames. Proc Combust Inst 2015;35(2):1735–43. https://doi.org/10.1016/j.proci.2014.06.137.

[32] Bhagatwala A, Luo Z, Shen H, Sutton JA, Lu T, Chen JH. Numerical and experimental investigation of turbulent DME jet flames. Proc Combust Inst 2015; 35(2):1157–66. https://doi.org/10.1016/j.proci.2014.05.147.

[33] Zhao Z, Chaos M, Kazakov A, Dryer FL. Thermal Decomposition Reaction and a Comprehensive Kinetic Model of Dimethyl Ether. Int J Chem Kinet 2008;40(1): 1–18. https://doi.org/10.1002/kin.v40:110.1002/kin.20285.

[34] Lu T, Law CK. A directed relation graph method for mechanism reduction. Proc Combust Inst 2005;30(1):1333–41. https://doi.org/10.1016/j.proci.2004.08.145.

[35] Zheng XL, Lu TF, Law CK. Experimental counterflow ignition temperatures and reaction mechanisms of 1,3-butadiene. Proc Combust Inst 2007;31(1):367–75. https://doi.org/10.1016/j.proci.2006.07.182.

[36] Sankaran R, Hawkes ER, Chen JH, Lu T, Law CK. Structure of a spatially developing turbulent lean methane-air Bunsen flame. Proc Combust Inst 2007;31 (1):1291–8. https://doi.org/10.1016/j.proci.2006.08.025.

[37] Burke U, Somers KP, O'Toole P, Zinner CM, Marquet N, Bourque G, et al. An ignition delay and kinetic modeling study of methane, dimethyl ether, and their mixtures at high pressures. Combust Flame 2015;162(2):315–30. https://doi.org/10.1016/j.combustflame.2014.08.014.

[38] Metcalfe WK, Burke SM, Ahmed SS, Curran HJ. A hierarchical and comparative kinetic modeling study of C1–C2 hydrocarbon and oxygenated fuels. Int J Chem Kinet 2013;45(10):638–75. https://doi.org/10.1002/kin.20802.

[39] Dames EE, Rosen AS, Weber BW, Gao CW, Sung C-J, Green WH. A detailed combined experimental and theoretical study on dimethyl ether/propane blended oxidation. Combust Flame 2016;168:310–30. https://doi.org/10.1016/j.combustflame.2016.02.021.

[40] Zeng M, Wullenkord J, Graf I, Kohse-Höinghaus K. Influence of dimethyl ether and diethyl ether addition on the flame structure and pollutant formation in premixed iso-octane flames. Combust Flame 2017;184:41–54. https://doi.org/10.1016/j.combustflame.2017.05.028.

[41] Curran HJ, Pitz WJ, Westbrook CK, Callahan GV, Dryer FL. Oxidation of automotive primary reference fuels at elevated pressures. Proc Combust Inst 1998;27(1):379–87. https://doi.org/10.1016/S0082-0784(98)80426-8.

[42] Mehl M, Pitz WJ, Westbrook CK, Curran HJ. Kinetic modeling of gasoline surrogate components and mixtures under engine conditions. Proc Combust Inst 2011;33(1):193–200. https://doi.org/10.1016/j.proci.2010.05.027.

[43] Curran HJ, Gaffuri P, Pitz WJ, Westbrook CK. A comprehensive modeling study of iso-octane oxidation. Combust Flame 2002;129:253–80. https://doi.org/10.1016/S0010-2180(01)00373-X.

[44] Andrae JCG. Development of a detailed kinetic model for gasoline surrogate fuels. Fuel 2008;87(10-11):2013–22. https://doi.org/10.1016/j.fuel.2007.09.010.

[45] K.V. Puduppakkam C.V. Naik C. Wang E. Meeks Validation studies of a detailed kinetics mechanism for diesel and gasoline surrogate fuels SAE Tech. Pap. 2010 p. 2010–01–0545 10.4271/2010-01-0545.

[46] Cai L, Pitsch H. Optimized chemical mechanism for combustion of gasoline surrogate fuels. Combust Flame 2015;162(5):1623–37. https://doi.org/10.1016/j.combustflame.2014.11.018.

[47] Mehl M, Chen JY, Pitz WJ, Sarathy SM, Westbrook CK. An approach for formulating surrogates for gasoline with application toward a reduced surrogate mechanism for CFD engine modeling. Energy Fuels 2011;25(11):5215–23. https://doi.org/10.1021/ef201099y.

[48] S.D. Givler M. Raju E. Pomraning P.K. Senecal N. Salman R. Reese Gasoline combustion modeling of direct and port-fuel injected engines using a reduced chemical mechanism SAE Tech. Pap. 2013 p. 2013–01–1098 10.4271/2013-01-1098.

[49] Wolk B, Chen J-Y. Computational study of partial fuel stratification for HCCI engines using gasoline surrogate reduced mechanism. Combust Sci Technol 2014;186(3):332–54. https://doi.org/10.1080/00102202.2013.870161.

[50] Chen Y, Wolk B, Mehl M, Cheng WK, Chen JY, Dibble RW. Development of a reduced chemical mechanism targeted for a 5-component gasoline surrogate: A case study on the heat release nature in a GCI engine. Combust Flame 2017;178: 268–76. https://doi.org/10.1016/j.combustflame.2016.12.018.

[51] Dagaut P, Daly C, Simmie JM, Cathonnet M. The oxidation and ignition of dimethylether from low to high temperature (500–1600 K): Experiments and kinetic modeling. Symp. Combust. 1998;27(1):361–9. https://doi.org/10.1016/S0082-0784(98)80424-4.

[52] Curran HJ, Pitz WJ, Westbrook CK, Dagaut P, Boettner JC, Cathonnet M. A wide range modeling study of dimethyl ether oxidation. Int J Chem Kinet 1998;30: 229–41. https://doi.org/10.1002/(SICI)1097-4601(1998)30:3<229::AID-KIN9>3.0.CO;2-U.

[53] Eldeeb MA, Akih-Kumgeh B. Investigation of 2,5-dimethyl furan and iso-octane ignition. Combust Flame 2015;162(6):2454–65. https://doi.org/10.1016/j.combustflame.2015.02.013.

[54] Zhang Y, El-Merhubi H, Lefort B, Le Moyne L, Curran HJ, Kéromnès A. Probing the low-temperature chemistry of ethanol via the addition of dimethyl ether. Combust Flame 2018;190:74–86. https://doi.org/10.1016/j.combustflame.2017.11.011.

[55] Mestas P, Clayton P, Niemeyer K. PyMARS: automatically reducing chemical kinetic models in Python. J Open Source Softw 2019;4:1543. https://doi.org/10.21105/joss.01543.

[56] Wang Hu, Yao M, Reitz RD. Development of a reduced primary reference fuel mechanism for internal combustion engine combustion simulations. Energy Fuels 2013;27(12):7843–53. https://doi.org/10.1021/ef401992e.

[57] Wang Hu, Yao M, Yue Z, Jia M, Reitz RD. A reduced toluene reference fuel chemical kinetic mechanism for combustion and polycyclic-aromatic hydrocarbon predictions. Combust Flame 2015;162(6):2390–404. https://doi.org/10.1016/j.combustflame.2015.02.005.

[58] Wang Hu, Deneys Reitz R, Yao M, Yang B, Jiao Qi, Qiu Lu. Development of an n-heptane-n-butanol-PAH mechanism and its application for combustion and soot prediction. Combust Flame 2013;160(3):504–19. https://doi.org/10.1016/j.combustflame.2012.11.017.

[59] Slavinskaya NA, Riedel U, Dworkin SB, Thomson MJ. Detailed numerical modeling of PAH formation and growth in non-premixed ethylene and ethane flames. Combust Flame 2012;159(3):979–95. https://doi.org/10.1016/j.combustflame.2011.10.005.

[60] Yang S, Wang Q, Curran HJ, Jia M. Development of a 5-component gasoline surrogate model using recent advancements in the detailed H2/O2/CO/C1-C3 mechanism for decoupling methodology. Fuel 2021;283:118793. https://doi.org/10.1016/j.fuel.2020.118793.

[61] Dirrenberger P, Glaude PA, Bounaceur R, Le Gall H, da Cruz AP, Konnov AA, et al. Laminar burning velocity of gasolines with addition of ethanol. Fuel 2014;115: 162–9. https://doi.org/10.1016/j.fuel.2013.07.015.

[62] Hirasawa T, Sung CJ, Joshi A, Yang Z, Wang H, Law CK. Determination of laminar flame speeds using digital particle image velocimetry: Binary fuel blends of ethylene, n-butane, and toluene. Proc Combust Inst 2002;29(2):1427–34. https://doi.org/10.1016/S1540-7489(02)80175-4.

[63] Egolfopoulos FN, Hansen N, Ju Y, Kohse-Höinghaus K, Law CK, Qi F. Advances and challenges in laminar flame experiments and implications for combustion chemistry. Prog Energy Combust Sci 2014;43:36–67. https://doi.org/10.1016/j.pecs.2014.04.004 Review.

[64] Andrae JCG, Brinck T, Kalghatgi GT. HCCI experiments with toluene reference fuels modeled by a semidetailed chemical kinetic model. Combust Flame 2008; 155(4):696–712. https://doi.org/10.1016/j.combustflame.2008.05.010.

[65] Song Yu, He Y, Yu Yi, Moreau B, Foucher F. Effect of Exhaust Gas Recirculation and NO on Ignition Delay Times of Iso-octane in a Rapid Compression Machine. Energy Fuels 2020;34(7):8788–95. https://doi.org/10.1021/acs.energyfuels.0c0078510.1021/acs.energyfuels.0c00785.s001.

[66] Rao VS, Skinner GB. Formation of D atoms in the pyrolysis of toluene-d8 behind shock waves. Kinetics of the reaction C7D8 + H → C7D7H + D. J Phys Chem 1984;88:4362–5. https://doi.org/10.1021/j150663a035.

[67] Goodwin DG, Speth RL, Moffat HK, Weber BW. Cantera: An Object-Oriented Software Toolkit For Chemical Kinetics, Thermo- Dynamics. And Transport Processes 2018. https://doi.org/10.5281/zenodo.1174508.

[68] Minetti R, Carlier M, Ribaucour M, Therssen E, Sochet LR. Comparison of oxidation and autoignition of the two primary reference fuels by rapid compression. Symp Combust 1996;26(1):747–53. https://doi.org/10.1016/S0082-0784(96)80283-9.

[69] Oehlschlaeger MA, Davidson DF, Herbon JT, Hanson RK. Shock Tube Measurements of Branched Alkane Ignition Times and OH Concentration Time Histories. Int J Chem Kinet 2003;36(2):67–78. https://doi.org/10.1002/(ISSN)1097-460110.1002/kin.v36:210.1002/kin.10173.

[70] Curran HJ. Developing detailed chemical kinetic mechanisms for fuel combustion. Proc Combust Inst 2019;37:57–81. https://doi.org/10.1016/j.proci.2018.06.054.

[71] C.K. Law Combustion physics 2006 Cambridge University Press Cambridge 10.1017/CBO9780511754517.

[72] Battin-Leclerc F. Detailed chemical kinetic models for the low-temperature combustion of hydrocarbons with application to gasoline and diesel fuel surrogates. Prog Energy Combust Sci 2008;34:440–98. https://doi.org/10.1016/j.pecs.2007.10.002.

[73] AlAbbad M, Javed T, Khaled F, Badra J, Farooq A. Ignition delay time measurements of primary reference fuel blends. Combust Flame 2017;178: 205–16. https://doi.org/10.1016/j.combustflame.2016.12.027.

[74] Di H, He X, Zhang P, Wang Z, Wooldridge MS, Law CK, et al. Effects of buffer gas composition on low temperature ignition of iso-octane and n-heptane. Combust Flame 2014;161(10):2531–8. https://doi.org/10.1016/j.combustflame.2014.04.014.

[75] Javed T, Lee C, AlAbbad M, Djebbi K, Beshir M, Badra J, et al. Ignition studies of n-heptane/iso-octane/toluene blends. Combust Flame 2016;171:223–33. https://doi.org/10.1016/j.combustflame.2016.06.008.

[76] Zhang Y, Somers KP, Mehl M, Pitz WJ, Cracknell RF, Curran HJ. Probing the antagonistic effect of toluene as a component in surrogate fuel models at low temperatures and high pressures. A case study of toluene/dimethyl ether mixtures. Proc Combust Inst 2017;36:413–21. https://doi.org/https://doi.org/10.1016/j.proci.2016.06.190.

[77] Lu L, Zou C, Lin Q, Liu Y, Jing H. Experimental and simulated study on the ignition delay time of dimethyl ether/n-heptane/oxygen/argon mixtures. Fuel 2020;264:116812. https://doi.org/10.1016/j.fuel.2019.116812.

[78] Gao Z, Hu E, Xu Z, Yin G, Huang Z. Effect of 2,5-dimethylfuran addition on ignition delay times of n-heptane at high temperatures. Front Energy 2019;13(3): 464–73. https://doi.org/10.1007/s11708-019-0609-z.

[79] Dmitriev AM, Knyazkov DA, Bolshova TA, Shmakov AG, Korobeinichev OP. The effect of methyl pentanoate addition on the structure of premixed fuel-rich n-heptane/toluene flame at atmospheric pressure. Combust Flame 2015;162(5): 1964–75. https://doi.org/10.1016/j.combustflame.2014.12.015.

[80] Zhao Z, Conley JP, Kazakov A, Dryer FL. Burning Velocities of Real Gasoline Fuel at 353 K and 500 K. SAE Tech. Pap., SAE. International 2003. https://doi.org/10.4271/2003-01-3265.

[81] Liao YH, Roberts WL. Laminar Flame Speeds of Gasoline Surrogates Measured with the Flat Flame Method. Energy Fuels 2016;30:1317–24. https://doi.org/10.1021/acs.energyfuels.5b01433.

[82] Mannaa O, Mansour MS, Roberts WL, Chung SH. Laminar burning velocities at elevated pressures for gasoline and gasoline surrogates associated with RON. Combust Flame 2015;162:2311–21. https://doi.org/10.1016/j.combustflame.2015.01.004.

[83] Wang Z, Wang S, Whiddon R, Han X, He Y, Cen K. Effect of hydrogen addition on laminar burning velocity of CH4/DME mixtures by heat flux method and kinetic modeling. Fuel 2018;232:729–42. https://doi.org/10.1016/j.fuel.2018.05.146.

[84] Frenklach M, Wang H. Detailed modeling of soot particle nucleation and growth. Symp Combust 1991;23(1):1559–66. https://doi.org/10.1016/S0082-0784(06)80426-1.

[85] Bhattacharya A, Basu S. An investigation into the heat release and emissions from counterflow diffusion flames of methane/dimethyl ether/hydrogen blends in air. Int J Hydrogen Energy 2019;44(39):22328–46. https://doi.org/10.1016/j.ijhydene.2019.06.190.

[86] Lokachari N, Burke U, Ramalingam A, Turner M, Hesse R, Somers KP, et al. New experimental insights into acetylene oxidation through novel ignition delay times, laminar burning velocities and chemical kinetic modelling. Proc Combust Inst 2019;37(1):583–91. https://doi.org/10.1016/j.proci.2018.07.027.

[87] Zhou C-W, Li Y, Burke U, Banyon C, Somers KP, Ding S, et al. An experimental and chemical kinetic modeling study of 1,3-butadiene combustion: Ignition delay time and laminar flame speed measurements. Combust Flame 2018;197:423–38. https://doi.org/10.1016/j.combustflame.2018.08.006.

[88] Inal F, Senkan SM. Effects of equivalence ratio on species and soot concentrations in premixed n-heptane flames. Combust Flame 2002;131(1-2):16–28. https://doi.org/10.1016/S0010-2180(02)00388-7.

[89] Shao C, Wang H, Atef N, Wang Z, Chen B, Almalki M, et al. Polycyclic aromatic hydrocarbons in pyrolysis of gasoline surrogates (n-heptane/iso-octane/toluene. Proc Combust Inst 2019;37(1):993–1001. https://doi.org/10.1016/j.proci.2018.06.087.

[90] Singh E, Badra J, Mehl M, Sarathy SM. Chemical Kinetic Insights into the Octane Number and Octane Sensitivity of Gasoline Surrogate Mixtures. Energy Fuels 2017;31(2):1945–60. https://doi.org/10.1021/acs.energyfuels.6b0265910.1021/acs.energyfuels.6b02659.s001.

[91] Singh E, Sarathy SM. The Role of Intermediate-Temperature Heat Release in Octane Sensitivity of Fuels with Matching Research Octane Number. Energy Fuels 2021;35(5):4457–77. https://doi.org/10.1021/acs.energyfuels.0c03883.

[92] vom Lehn F, Cai L, Tripathi R, Broda R, Pitsch H. A property database of fuel compounds with emphasis on spark-ignition engine applications. Appl Energy Combust Sci 2021;5:100018. https://doi.org/10.1016/j.jaecs.2020.100018.

[93] Sarathy SM, Kukkadapu G, Mehl M, Javed T, Ahmed A, Naser N, et al. Compositional effects on the ignition of FACE gasolines. Combust Flame 2016; 169:171–93. https://doi.org/10.1016/j.combustflame.2016.04.010.

[94] Bhattacharya A, Datta A. Laminar burning velocity of biomass-derived fuels and its significance in combustion devices. Green Energy Technol. 2018:359–78. https://doi.org/10.1007/978-981-10-8393-8_16.

[95] Chu H, Ya Y, Nie X, Zhou Y, Hu J, Dong S, et al. Effects of ethanol and 2, 5-dimethylfuran addition on the morphology and nanostructure evolution of soot in gasoline primary reference fuel-air coflow diffusion flames. Fuel 2020;281: 118711. https://doi.org/10.1016/j.fuel.2020.118711.

[96] Poinsot T, Veynante D, Candel S. Quenching processes and premixed turbulent combustion diagrams. J Fluid Mech 1991;228:561–606. https://doi.org/10.1017/S0022112091002823.

[97] Hansen N, Miller JA, Kasper T, Kohse-Höinghaus K, Westmoreland PR, Wang J, et al. Benzene formation in premixed fuel-rich 1,3-butadiene flames. Proc Combust Inst 2009;32(1):623–30.

[98] Xu L, Yan F, Dai W, Zhou M, Chung SH, Wang Y. Synergistic effects on soot formation in counterflow diffusion flames of acetylene-based binary mixture fuels. Combust Flame 2020;216:24–8. https://doi.org/10.1016/j.combustflame.2020.02.013.

[99] Kalghatgi GT, Bradley D. Pre-ignition and "super-knock" in turbo-charged spark-ignition engines. Int J Engine Res 2012;13(4):399–414. https://doi.org/10.1177/1468087411431890.

[100] Fagundez JLS, Sari RL, Garcia A, Pereira FM, Martins MES, Salau NPG. A chemical kinetics based investigation on laminar burning velocity and knock occurrence in a spark-ignition engine fueled with ethanol–water blends. Fuel 2020;280:118587. https://doi.org/10.1016/j.fuel.2020.118587.

[101] Kalghatgi G, Babiker H, Badra J. A Simple Method to Predict Knock Using Toluene, N-Heptane and Iso-Octane Blends (TPRF) as Gasoline Surrogates. SAE Int J Engines 2015;8:505–19. https://doi.org/10.4271/2015-01-0757.

[102] Bhattacharya A, Banerjee DK, Mamaikin D, Datta A, Wensing M. Effects of Exhaust Gas Dilution on the Laminar Burning Velocity of Real-World Gasoline Fuel Flame in Air. Energy Fuels 2015;29(10):6768–79. https://doi.org/10.1021/acs.energyfuels.5b01299.

[103] Badra JA, Bokhumseen N, Mulla N, Sarathy SM, Farooq A, Kalghatgi G, et al. A methodology to relate octane numbers of binary and ternary n-heptane, iso-octane and toluene mixtures with simulated ignition delay times. Fuel 2015;160:458–69. https://doi.org/10.1016/j.fuel.2015.08.007.